GRANT/manuscript
64 pages

IN-21910

FINAL TECHNICAL REPORT

National Aeronautics and Space Administration Grant NAG8-433

A Study of the Discrepant QSO X-ray Luminosity Function from the HEAO-2 Data Archive

Principal Investigator:

Professor Bruce Margon

Department of Astronomy, FM-20

University of Washington

Seattle, Washington 98195

I. INTRODUCTION

Although studied intensively for more than 20 years (*e.g.*, Giacconi *et al.* 1962), the origin of the diffuse X-ray background radiation (hereafter, XRB) above ~1 keV remains controversial. The most popular explanations are thermal bremsstrahlung from a hot intergalactic medium, with density perhaps of order the closure density, or the superposition of a large number of discrete X-ray sources (*e.g.*, Setti and Woltjer 1979). Strong support for the latter explanation has come from observations by the *Einstein Observatory*. The most sensitive *Einstein* X-ray images (the "Deep Survey" fields) resolve, by direct integration of the X-ray log N-log S curve, $26 \pm 11\%$ of the XRB into discrete sources (Giacconi *et al.* 1979*b*). Unfortunately, the limiting sensitivity of these deepest of all currently available X-ray exposures leaves $\sim 75\%$ of the XRB unresolved.

Einstein observations also strongly confirmed that QSOs were a prime candidate class for that discrete source contribution (*e.g.*, Tananbaum *et al.* 1979). Thus a second approach to estimate the discrete source contribution to the XRB has been to use the QSO optical log N-log S curve, and a relation (*e.g.*, the mean luminosity ratio $< L_x/L_{opt} >$) which allows one to predict QSO X-ray emission from that in the optical (*e.g.*, Zamorani *et al.* 1981). Although this latter approach is much less direct, potentially it can be used to estimate the the contribution of all QSOs, even very faint ones, to the XRB. In order to use this optical log N-log S approach, we need to know the X-ray properties of "typical" QSOs. By "typical", we mean QSOs of apparent optical magnitude (and hence, X-ray flux and surface density on the sky) potentially capable of contributing substantially to the XRB. Unfortunately, the overwhelming majority of previous observations of QSOs with *Einstein* fall into two categories, neither of which are "typical".

The first such category is the targeted observations of heterogeneous collections of previously known QSOs, many of which are famous for being *atypically* bright in the optical and/or radio (*e.g.*, Zamorani *et al.* 1981: Ku, Helfand, and Lucy 1980). Although

complicating their direct use in the optical log N-log S approach, the heterogeneity (in z, B, L_{opt}, L_{rad}, selection, etc.) of such collections has led to the realization that $< L_x/L_{opt} >$ is not constant for all types of QSOs. In addition to a significant dependence on radio properties (Tananbaum *et al.* 1983), $< L_x/L_{opt} >$ has been found to depend on L_{opt} and/or z such that higher redshift and/or higher optical luminosity QSOs have smaller $< L_x/L_{opt} >$ ratios (Avni and Tananbaum 1982). An issue of much current controversy, and critically important for proper use of the optical log N-log S approach, is which of these dependences (L_{opt} or z) is primary (see § 5). Because of such dependences on L_{opt} and/or z, ensemble distribution parameters such as $< L_x/L_{opt} >$ are, in fact, directly interpretable quantities only for a sample of QSOs which includes a narrow range of values of L_{opt} and/or z: such a narrow sample might be used to emprically test various models (suggested by the broad samples) for the dependence of $< L_x/L_{opt} >$ on L_{opt} and/or z.

A second category of *Einstein* observed QSOs are the X-ray selected samples (*e.g.*, Margon, Downes, and Chanan 1985; Gioia *et al.* 1984, and references therein). However, these X-ray selected samples can yield only limited information about typical QSOs; at the risk of stating the obvious, X-ray selection tends to preferentially select the X-ray bright objects. Further, the dependence of $< L_x/L_{opt} >$ on L_{opt} and/or z results in a mean redshift for X-ray selected samples of only $z \leq 0.6$, and such low redshift QSOs are too rare to contribute substantially to the XRB.

More recently, however, several X-ray studies of *homogeneous* optically selected samples of QSOs have been discussed by Marshall *et al.* (1984), Anderson (1985; hereafter "A85"), Kriss and Canizares (1985), Tananbaum *et al.* (1986), Avni and Tananbaum (1986), and Schmidt and Green (1986). These last three papers report on X-ray observations of the "XBQS", an *Einstein* observed subset of $\sim$ 60 QSOs from the Bright Quasar Sample (BQS) of Schmidt and Green (1983). The XBQS is very important because of its unique position in the L_{opt}, z plane, as well as the high X-ray detection fraction ($\geq$ 80%). However, the

$B \leq 16$ QSOs of the sort studied in the XBQS are themselves much too rare to contribute substantially to the XRB. Because the BQS is a UV-excess selected sample, it is complete only for $z < 2.2$. Kriss and Canizares (1985) obtained deep *Einstein* images of two fields in which Hoag and Smith (1977) and Sramek and Weedman (1978) had previously grism-selected 22 QSOs, most at high redshift. Marshall (1983) obtained deep *Einstein* images of the "Braccesi Faint" (hereafter, BF) sample of $\sim$ 35 QSOs (Formiggini *et al.* 1980). The BF is a UV-excess selected sample complete for $B \leq 19.8$ and $z < 2.2$. Thus, although the literature contains X-ray information on hundreds of QSOs, X-ray data have been reported for only a single complete sample of optically selected QSOs – the 35 objects of the BF sample – of the sort that might contribute substantially to the XRB, and there have been no such studies of large, complete samples of typical high redshift QSOs. As we shall discuss below, X-ray observed complete samples of optically selected QSOs can be used with very few uncertain extrapolations to estimate the contribution of such QSOs to the XRB.

In summary, previous data on X-ray emission from typical QSOs lacked the following: (1) a narrow sample (in $L_{opt} - z$ space) to aid in testing empirically the various previously-suggested models for the dependence of $< L_x/L_{opt} >$ on L_{opt} and/or z; and, (2) a large, complete sample at high redshift to complement the BF sample. In order to obtain such samples of typical QSOs, we have taken, in an "after the fact" fashion, grism/grens plates of $\sim$ 17 deg^2 of the sky previously imaged to very sensitive X-ray flux levels with the *Einstein Observatory*. The archived X-ray data for our study includes 50 Imaging Proportional Counter (IPC) fields and five High Resolution Imager (HRI) fields which have among the longest integration times of all *Einstein* images. The new optical data, obtained at various 4m class telescopes, include at least one "blue grism/grens" plate centered on each of these same deep X-ray fields. In this fashion, we have optically selected more than 400 previously uncataloged QSO candidates for which the most sensitive X-ray flux information is already extant. In this report, we will concentrate on a high redshift subsample ($\sim$ 90 objects) of

this larger data base for which grism/grens selection is highly efficient and reliable.

In § 2, we present details on the optical selection of our high redshift QSOs. Keeping in mind the motivations discussed above, we define two optical samples: a "complete" sample and a "narrow" sample. Section 3 presents a discussion of the X-ray data for these new samples. Because most of our QSOs are not detected in X-rays, it is necessary to incorporate information contained in X-ray non-detections as well as detections; two such statistical techniques, "stacking" and "survival analysis", and some cautions about their use are presented in § 4 and the Appendix. Finally, in § 5, we use our data to investigate the ensemble X-ray properties (*e.g.*, contribution to the XRB, dependence of $< L_x/L_{opt} >$ on L_{opt} and/or z, etc.) of high redshift QSOs, and the QSO population in general. A more detailed account of some of the research described herein may be found in A85, and preliminary results of this work have been reported by Anderson and Margon (1983, 1984, 1986).

II. THE OPTICAL SAMPLES

The grisms in use at the 4m telescopes of the Kitt Peak National Observatory and Cerro Tololo Interamerican Observatory, and the "grens" at the Canada-France-Hawaii Telescope, are particularly well suited to discovery surveys for strong emission line QSOs (Smith 1981, 1982). The fields of view of the grisms are about $34' \times 34'$. A CFHT grens plate covers about $54' \times 54'$; however, due to degradation of image quality near the field edges, combined with vignetting, and guide and calibration probe obscuration, the grens plates have an effective useful area of order 0.5 deg^2 (Weedman 1985; Crampton, Schade, and Cowley 1985). These fields of view are well matched to those of the *Einstein* X-ray images ($\approx 1^\circ \times 1^\circ$)

Centered on each of the 55 deep *Einstein* fields, which are scattered disjointly over the celestial sphere, we obtained a IIIaF+blue grism/grens plate combination as the primary

plate for selection of the QSO sample. The "blue grism" has a blaze wavelength of 3550 Å and linear reciprocal dispersion of 1500 Å mm^{-1}, while the "blue grens" has 1000 Å mm^{-1} dispersion with a blaze at 4000 Å. Our desire to obtain redshifts directly from the plate material was a primary motivation for choosing the IIIaF, with its wider wavelength coverage of 3200 Å-6900 Å, rather than the IIIaJ emulsion. Wavelengths of strong emission features are estimated from the grism/grens plates to an accuracy of $\sim$ 100 Å. To extend sensitivity at redder wavelengths, we also obtained "red grism" (blaze $\sim$ 6000 Å) plates on either a IIIaF emulsion, or on a IV-N emulsion (6100-8900 Å with a blue-cut Wratten 29 filter) whenever time permitted (about 20 fields). In order to maintain as uniform a sample as possible for the current study, these red grism plates are used only as additional confirmation of the candidate as a QSO, or to confirm the redshift, but not for selection. Typically, sky-limited exposures are $\approx 45 - 60$ min on baked IIIaF plates, and reach a limiting continuum magnitude of $B \approx 21.0$; exposure times are 60-90 min on the IV-N plates hypersensitized in silver nitrate, and reach a similar limiting magnitude in V.

The plates were scanned visually using a binocular microscope and an "underlay" grid to systematize the search. Both emission line QSO candidates (the main thrust of this report) and UV excess objects were searched for. In the $\approx$ 17 deg^2 (effective area) of sky surveyed, approximately 400 QSO candidates were selected. Each plate was searched several times at separate sessions, and the thoroughness of our search may be addressed through the following considerations. A typical limiting continuum magnitude for a blue grism+IIIaF plate taken at a 4m telescope in better than 2″ seeing is $B \approx 20.5$ (Clowes 1981). Thirty previously known QSOs (of all redshifts) from the catalog of Véron-Cetty and Véron (1985) lie within the area surveyed by our "high quality" plates (all grens plates and 38 grism fields, all taken in $\leq 2''$ seeing), and have $B < 20.5$; only 8 (27%) were not successfully recovered in our "double blind" searches of the plates. More importantly, in the redshift regime where grism/grens selection is most successful ($z \geq 1.8$), *all* seven of the

previously known high redshift QSOs with $B < 20.5$ were not only recovered in this fashion, but also were assigned the proper redshift. The success with which the previously known high redshift QSOs with $B < 20.5$ were recovered provides considerable confidence in the thoroughness of our search technique, to ≈ 1 magnitude fainter than the completeness limit for which we will argue below. Previously catalogued QSOs which are also the targets of the *Einstein* X-ray images are excluded from the optically selected samples to be defined below, even if successfully recovered. This is necessary to avoid potential X-ray biases of the sort discussed in the introduction.

In examining our plates, we have found ~ 200 low redshift ($z < 1.8$) QSO candidates to $B \leq 20$ which have strong UV excess (UVX), but which lack any obvious emission features. We expect that ~ 100 of these are indeed low redshift QSOs (see arguments in A85), and roughly 40 such objects are the likely optical identifications of *Einstein* serendipitous X-ray sources. However, pending follow up spectroscopy and completeness studies, these UV excess objects will not be discussed further.

a) The Emission Line Candidates

There are redshift and magnitude regimes where grism/grens selection is particularly efficient and the plates themselves can, with reasonable confidence, be used to classify the candidates as QSOs, and estimate redshifts. The efficiency with which emission line objects are selected from grism/grens plates depends strongly on line strength and the seeing, as well as on the continuum magnitude. The dependence on line strength highly favors the selection of "Lyman-α" QSOs at $z \geq 1.8$, where Lα is redshifted onto the wavelength response of the IIIaF emulsion. With the grism/grens, the spectral resolution is determined by the seeing. All CFHT plates were taken in $< 1''$ seeing (resolution ~ 70 Å), and we were able to obtain a blue grism plate in $\leq 2''$ seeing for almost all the grism fields (resolution better than ~ 150 Å). The frequently excellent seeing at the CFHT, coupled with the higher dispersion of the grens, allows somewhat weaker-lined objects to

be detected than with the grism (Crampton, Schade, and Cowley 1985).

The non-uniform response of the IIIaF emulsion as function of wavelength is well known. In combination with the blue grism, qualitatively the response is as follows (see also Fig. 1 of Carswell and Smith 1978): there is a broad maximum near 3500 Å with nearly smoothly decreasing sensitivity to 4800 Å; redward of 4800 Å there are peaks in the response at 5300 Å, 6100 Å, and 6800 Å. Because these response peaks can sometimes be confused with emission lines, we henceforth will concentrate only on QSOs selected from blue grism/grens plates which have an obvious strong feature blueward of 4800 Å, corresponding corresponding to $z < 3.0$ for Lα QSOs. The additional spectral information redward of 4800 Å is used in the current application only to look for confirming spectral features.

b) The Complete Sample "C"

Clowes (1981) has given a quantitative discussion of selection effects operating in grism surveys, concentrating especially on the blue-grism plus IIIaF combination. Clowes' models predict, for example, a selection curve for the IIIaF+blue grism plates which provides a description of how the plate limiting equivalent width of Lα+N V varies as a function of seeing and continuum magnitude. Clowes' models are quite successful at reproducing the appropriate data from the Hoag and Smith grism survey (Hoag and Smith 1977; Osmer 1980).

The distribution of rest frame Lα+N V equivalent widths is available for a large sample of radio-selected QSOs (Wilkes 1986). For all blue-grism plates taken in $\leq 2''$ seeing (38 fields), we have used Clowes' models to estimate the limiting equivalent width of Lα+N V detectable to an (observed) magnitude of $B \leq 19.5$. Then, by comparing these values with Wilkes' equivalent width distribution, we estimate that our sample of Lα QSOs from these 38 plates should be $\geq 80\%$ complete. A radio selected sample is appropriate for this comparison because radio selection is the only efficient line-strength-independent technique

of finding high-redshift objects.

Further confirmation that significant incompleteness sets in at $B > 19.5$ is provided in Figure 1, in which we display the apparent magnitude distribution for the high redshift QSO candidates in our sample. Because the surface density of grism selected QSOs per unit magnitude is thought to not decrease until magnitudes of order $B \sim 20.5$ (Gaston 1983), the paucity of QSOs to the faint side of the peak of the figure is likely attributable to the onset of incompleteness.

Thus, we have established a subsample (hereafter, the "complete sample", or sample "C") of our emission line selected QSOs which should constitute a reasonably complete ($\geq 80\%$) sample. Sample C consists of all emission line QSOs with $1.8 \leq z \leq 3.0$ and $B \leq 19.5$ selected from our high quality blue grism plates. When only a single line is detected on the plate (true for about half of the objects), we have assumed the line identification to be Lα; other workers (*e.g.*, Osmer 1980) have found that $\sim 80\%$ of such strong-lined grism objects indeed turn out to be Lα QSOs. We argue later that this assumption is also a conservative approach when interpreting the contribution of QSOs to the X-ray background. For uniformity in optical selection biases, we exclude from sample C those QSOs selected on other plate-grism/grens combinations.

The 38 fields for which high quality blue grism+IIIaF plates are available cover an area of 12.9 deg^2; 39 sample C objects were found in these fields, yielding a surface density of 3.02 ± 0.48 QSOs deg^{-2} to $B = 19.5$, with redshifts $1.8 \leq z \leq 3.0$. The 39 QSOs of sample C are listed in Table 1. The surface density found here is in good agreement with that found by other workers; for example, a value of ≈ 2.7 was found in the Hoag and Smith survey using the same grism/emulsion combination (see discussion in Schmidt and Green 1983). The "complete" sample C will be used in § 5 for a direct estimation of the contribution of such high redshift QSOs to the XRB.

c) The Narrow Sample "N"

The second subsample of objects we define (hereafter, the "narrow" sample, or sample "N"), includes 79 emission line QSOs selected from *both* high quality grens and grism plates, which also fall within the following parameter ranges ranges: $1.8 \leq z \leq 2.5$ and $31.0 \leq \log l_{2500} \leq 32.0$, where l_{2500} (in units of erg s^{-1} Hz^{-1}) is the monochromatic luminosity at 2500 Å in the QSO frame. Sample N does not constitute a complete sample, but merely represents those QSOs candidates for which the plate material alone is deemed adequate to confidently classify the object as a QSO, and which lie in a narrow redshift and magnitude (and hence, optical luminosity) range where grism/grens selection is highly efficient.

In addition, we have also included in sample N another ten QSOs from the the Kriss and Canizares (1985) study which also lie within the sample N parameter ranges. These latter QSOs were discovered with the identical blue grism used in our study. Sample N, then, includes a total of 89 objects which occupy a narrow region of $L_{opt} - z$ space. Although incomplete, this sample is nevertheless well suited for empirically testing models for the dependence of $< L_x/L_{opt} >$ on such other parameters as L_{opt} and z, *i.e.*, for studying the X-ray conditional luminosity function (see, *e.g.*, Avni and Tananbaum 1982, 1986).

The QSOs of sample N have means of optical luminosity and redshift of, respectively, $< \log (l_{2500}) >= 31.44$, and $< z >= 2.1$, and a listing of the objects is given in Table 2. There are 30 objects in common between the samples N and C.

d) Optical Magnitudes and Monochromatic Luminosities at 2500 Å

In order to determine the ratio L_x/L_{opt}, we need to estimate l_{2500} for these QSOs. Optical B magnitudes are estimated using image diameter measurements from the Palomar Observatory *Sky Survey O* print, and converted to B magnitudes using the approach outlined in Hayman, Hazard, and Sanitt (1979). To avoid systematic biases (personal or instrumental), we recalibrated the image-diameter/magnitude relation for our own eye/50× microscope combination (A85). Two "photometric" standard fields were used

to test the reliability of our recalibrated image diameter-magnitude relation: the first includes 47 photoelectrically calibrated standards from a field in M15 (Sandage and Katem 1977), while the second includes the 53 grism selected QSOs (Sramek and Weedman 1978) with magnitudes determined from spectrophotometry and microdensitometry (Vaucher and Weedman 1980). For both these photometric test samples, the *rms* differences between our POSS estimates and the photometric ones are ≤ 0.5 mag for $B < 20.7$. These reliability test results are displayed in Figure 2 and clearly show that any systematic errors should be quite small in the mean (≤ 0.1 mag). Our estimates are considerably more uncertain ($rms \sim 1$ mag) at $B \geq 20.7$ (A85), and therefore in sample N only those objects with $B \leq 20.7$ are included.

The POSS B magnitudes are corrected to continuum magnitudes using the data in Véron (1983) to estimate the line contributions, ΔB(line), to the observed magnitude as a function of redshift. The magnitudes are further corrected for extinction within the Galaxy, using

$$\Delta B(\mathrm{ext}) = -0.24 \csc |b^{II}|. \qquad (1)$$

Finally, the corrected B magnitudes are converted to monochromatic luminosities at 2500 Å in the QSO rest frame using relations from Schmidt (1968), Schmidt and Green (1983), and Marshall (1983).

We have assumed a power law spectral form of energy index $\alpha_o = 1.0$ for the optical continuum, and adopt $q_0 = 0$, $H_0 = 50$ km s^{-1} Mpc^{-1} unless otherwise stated. These values are chosen mainly for ease of comparison with previous studies of the X-ray properties of QSOs (*e.g.*, Zamorani *et al.* 1981). The optical characteristics of samples C and N are shown in Tables 1 and 2. Note that we have revised the l_{2500} values for the ten Kriss and Canizares (1985) objects to our assumed $\alpha_o = 1.0$.

e) Optical Coordinates

Optical coordinates were measured from the POSS prints using several two-axis mea-

suring machines. Although accuracies differ among these machines, all optical coordinates should be accurate to at least 5″. Such accuracy is more than adequate for the IPC fields, but for the HRI with its ~ 3″ X-ray error circles, some of these optical coordinate uncertainties are larger than optimum. Optical coordinates for sample N and C QSOs are also listed in Tables 1 and 2. Finding charts for these QSOs are available in A85 or from the authors.

III. THE X-RAY DATA

The archived *Einstein* X-ray data for our study are IPC and HRI images which provide both spatial resolution and flux information for X-rays of energy a few keV. The IPC has a field of view of 60′ × 60′ (but with ~ 38′ × 38′ inside the window support "ribs"), and spatial resolution of ~ 1.5′. The HRI (field of view of 27′ × 27′) provides higher spatial resolution of 2″, but with comparatively low quantum efficiency.

The particular X-ray images chosen consist of high galactic latitude fields ($|b^{II}| > 20^{\circ}$) with very long integration times: 50 IPC images with integration times of 10,000–45,000 s, and five HRI images with integration times of 40,000–100,000 s. Thus, the fields we use overlap in sensitivity with the so-called "Deep Survey" fields, the handful of the very deepest *Einstein* X-ray images (30,000–60,000 s in the IPC, and 10,000–50,000 s in the HRI), and are among the most sensitive of any currently available.

These X-ray fields were initially imaged in X-rays for reasons not directly related to the current study, having instead, a wide range of potential X-ray sources as their primary targets, *e.g.*, bright stars, cataclysmic variables, clusters of galaxies, normal galaxies, and AGN/QSOs. However, the X-ray information on the target commonly is contained within only the central ≤ 2% of the area imaged. In an "after the fact fashion" (*i.e.*, after the X-ray data had already been acquired), we obtained grism/grens plates centered on these deep *Einstein* images. The X-ray properties of the optically selected samples C and N are investigated here using the "unused" portions of these X-ray images.

The approach used here is to be contrasted with programs aimed at the optical identification of serendipitous X-ray sources (*e.g.*, Margon, Downes, and Chanan 1985, Gioia *et al.* 1984, Kriss and Canizares 1982, Reichert *et al.* 1982). The latter approach results in an X-ray selected sample of objects. On the other hand, the QSOs investigated here are first *optically* selected from the grism/grens plates, and then the archived *Einstein* images are used to derive a sensitive X-ray flux detection, or more frequently, an X-ray flux upper limit. Our optically selected grism/grens samples have no *a priori* X-ray biases.

a) Source Detection Algorithms in the IPC

The IPC (Giacconi *et al.* 1979*a*, 1981) has non-negligible response to, as well as limited spectral resolution for, X-rays of energy 0.2-0.28 and 0.4-4.5 keV. In practice, the objects of Samples C and N have such low X-ray fluxes that the IPC must be used in broadband fashion. Thus, for the present study, IPC count rates and fluxes will generally be estimated for the broadband range 0.5–3.0 keV; however, several other broadband energy ranges are also used to ascertain source existence. The standard IPC production reprocessing (Harnden *et al.* 1984) has been applied to almost all the relevant fields, and includes an automated search technique (in several broad energy bands) to locate X-ray sources. For the present study, an optically selected QSO is considered to have been detected by the automated source finding algorithms provided that the total number of counts in a $2.4' \times 2.4'$ region equals or exceeds 5σ above that predicted for the background, assuming Poisson statistics.

We have also performed a second test for source existence with the IPC data, using a larger region of radius $3'$ centered on the optically selected QSO position; the background is estimated from a concentric annular "detect frame" extending radially from $3'$ to $5'$, and the 0.5–3.0 keV band is used. This circular detect region is sufficiently large that: (1) virtually all counts in the 0.5–3.0 keV band fall within the $3'$ circular region for a wide range of reasonable possible QSO X-ray spectra; (2) even if the X-ray centroid and the

optical position differ by $\sim 1'$, most of the X-ray counts will still fall within the region. This latter point is particularly important for "stacking" the images (see below) when the QSO is not obviously detected in X-rays. The price paid for using the larger $3'$ detect region is the introduction of extra background noise into the determination of source counts. For example, a 5σ detection of a QSO in the $2.4' \times 2.4'$ region would register only as a $\approx 2.6\sigma$ detection in the $3'$ radius circle. Thus, in addition to the 5σ automated detection algorithm criterion, we also count as possible detections QSOs which show a $\geq 2.6\sigma$ detection in the larger $3'$ circular region.

b) Fluxes in the IPC

For the reasons given above, broadband IPC count rates in the 0.5–3.0 keV band are also determined using the larger $3'$ circular detect region. Again, this introduces considerable additional background noise, and a few of the weaker sources (even though 5σ detections in the automated source finding algorithms) have rather large (to $\sim 50\%$) uncertainties in their count rates (and hence fluxes). For objects not detected in X-rays, we derive a 2.6σ upper limit appropriate to the $3'$ radius region (corresponding to a 5σ upper limit in the automated detection algorithms).

The IPC broadband flux $F_{\rm obs}$ (0.5–3.0 keV) is derived from the observed source count rate as described by Tananbaum *et al.* (1979). We use a recent recalibration of the IPC effective area that causes the X-ray fluxes listed here to be systematically $\sim 10\%$ higher than the values which would have been found using the earlier calibration. In converting a broadband count rate into a broadband flux, it is necessary to assume an X-ray spectrum. Following the usual practice, (*e.g.*, Zamorani *et al.* 1981), we assume that the average QSO spectrum (in the 0.5–3.0 keV range) is a power law with spectral (energy) index $\alpha_x = 0.5$. This spectrum has been traditionally assumed for it is similar to the value 0.4 found for the spectrum of the XRB in the 3-20 keV band (Schwartz 1979); de Zotti *et al.* (1982) have shown that if the discrete source contribution to the XRB is substantial, the

typical contributors must have X-ray spectra within a few tenths of $\alpha_x = 0.5$. Further, such a spectrum is also similar to that of 3C 273 (Worrall *et al.* 1979). However, for lower luminosity AGN (particularly Seyfert 1s) the mean spectrum between 0.7 and 100 keV has spectral index $\alpha_x \sim 0.7 - 0.8$ (Mushotzky *et al.* 1980, Rothschild *et al.* 1983, Petre *et al.* 1984). Further, recent work (Elvis, Wilkes, and Tananbaum 1985, Elvis and Lawrence 1985) indicates that the mean value for a subset of the BQS may be much closer to $\alpha_x = 1.0 - 1.2$, with a wide dispersion about the mean. The XRB intensity is well measured only above ≈ 2 keV, and yet the IPC and HRI have an "effective" energy response of 1–2 keV; thus, it is common practice to compare *Einstein* and XRB data in terms of monochromatic fluxes at 2 keV. The response of the IPC is such that if the actual X-ray spectral slope is of order 1.2 rather than 0.5, the inferred monochromatic flux at 2 keV for a QSO, and the contribution of QSOs to the XRB at at 2 keV, will be overestimated by $\sim 40\%$. This unavoidable uncertainty may dominate our analysis, and we stress that we employ $\alpha_x = 0.5$ for conservatism and for consistency with previously published results. The combined uncertainties of α_x, variations in the IPC gain, and corrections for interstellar photoelectric opacity imply a total uncertainty in broadband fluxes of $\sim 30\%$ (Tananbaum *et al.* 1979).

c) The High Resolution Imager (HRI)

The HRI (Giacconi *et al.* 1979*a*, 1981) also provides broadband ($\sim 0.1 - 4.5$ keV) imaging and flux information. The HRI provides high spatial resolution ($\sim 2''$), but at the expense of spectral information, field of view, and sensitivity compared with the IPC. In the current application, the primary interest is to push to very faint X-ray flux levels, and so only a few very long integration HRI fields have been included in our survey. The lack of energy resolution in the HRI introduces added uncertainty into the conversion of count rates into monochromatic fluxes.

Similar analysis methods to those discussed above for the IPC were applied to the

HRI images. Sources found by the automated source finding algorithms are checked for positional coincidence of $\leq 5''$ (most of this uncertainty is due to the optical position uncertainty) with the sample C and N QSOs, and smoothed X-ray contour maps were made. Finally, we followed the approach outlined by Marshall (1983) as a further check. At the location of each optically selected QSO, we used a circular region (6.8″ radius for source $\leq 7'$ off axis, and 13.5″ for sources $\geq 10'$ off-axis) to establish source reality; proper allowance was made for optical position uncertainties, and the background was estimated from a nearby $4' \times 4'$ box which contains no obvious X-ray sources. A detection is again defined as 5σ above background in this circular region. As for the IPC images, HRI count rates and fluxes are estimated using a larger region (in this case an 18″ radius circle), again implying that some genuine sources have rather large uncertainties in their count rates and fluxes.

d) X-Ray Fluxes, Luminosities, and Luminosity Ratios for Grism/Grens Selected QSOs

Broadband X-ray fluxes (corrected for absorption in the Galaxy) are converted into monochromatic 2 keV luminosities, $l_{2\ keV}$, assuming $\alpha_x = 0.5$ and using the relations given in Zamorani *et al.* (1981). It is useful to compare the ratio of X-ray and optical monochromatic luminosities; this ratio is independent of uncertainties in the cosmological parameters H_0 and q_0, and allows for easy comparison of the relative X-ray emissivities of QSOs of a variety of optical luminosities. We follow the usual practice (*e.g.*, Tananbaum *et al.* 1979), and parameterize this ratio through the quantity α_{ox}, which is the slope of a hypothetical power law connecting optical (2500 Å) and X-ray (2 keV) wavebands in the QSO frame,

$$\alpha_{ox} = -\frac{\log\left(l_{2\ \mathrm{keV}}/l_{2500}\right)}{\log\left(\nu_{2\ \mathrm{keV}}/\nu_{2500}\right)} = -[\log\left(l_{2\ \mathrm{keV}}/l_{2500}\right)]/2.605. \qquad (2)$$

Presented in Table 3 are the X-ray data for sample C and N QSOs. Even at these

most sensitive of all currently available X-ray sensitivities, only $\sim 27\%$ (21/78 for sample N, and 10/37 for sample C) of the grism/grens selected objects are detected in X-rays. Note that a few sample C and N QSOs from § 2 do not lie within the X-ray image and are omitted from the table. The position angles of the X-ray image and the grism/grens plate are not identical, so that there are non-overlap regions in the corners, for example.

At the very sensitive X-ray and optical flux levels of our data, the chance of a positional coincidence between a grism/grens selected QSO and a physically unrelated X-ray source is non-negligible. Using the X-ray log N-log S curve from the Deep Survey study of Giacconi *et al.* (1979*b*), we predict that to a typical limiting sensitivity of 5×10^{-14} erg cm^{-2} s^{-1} (0.5-3.0 keV), there is of order one such chance coincidence within samples C and N.

Recalling that 43% of the comparably optically faint BF QSOs were detected in X-rays (Marshall 1983), the low rate of positive flux detections reported here gives the first qualitative indications that our high redshift objects might have lower ratios of X-ray to optical emissivities than their lower redshift/lower optical luminosity counterparts. One way to parameterize the mean X-ray to optical luminosity ratio of a sample of QSOs is the parameter $\alpha_{ox}^{\rm eff}$ (Tananbaum *et al.* 1979). By analogy with the definition of α_{ox} above, this parameter is defined as

$$\alpha_{ox}^{\rm eff} = -[\log < l_{2\,\rm keV}/l_{2500} >]/2.605. \qquad (3)$$

where $< l_{2\,\rm keV}/l_{2500} >$ is the mean of the $l_{2\,\rm keV}/l_{2500}$ ratio for the sample. Note that $\alpha_{ox}^{\rm eff}$ is not the same as the mean α_{ox}, $< \alpha_{ox} >$, which we also employ elsewhere. In order to determine these mean parameters for samples C and N, and quantitatively compare them with other samples, it is essential to use a statistical approach which incorporates information contained in the X-ray non-detections.

IV. TWO STATISTICAL APPROACHES FOR INCORPORATING INFORMATION IN X-RAY NON-DETECTIONS

In this section, we briefly discuss two techniques to deal with "censored" data, *i.e.*, data with some upper or lower limits. The first approach, "survival analysis", has been widely used in X-ray studies of QSOs. Survival analysis is powerful in the sense that it allows an estimation not only of single ensemble parameters like $\alpha_{ox}^{\rm eff}$, but also of, for example, the distribution function of α_{ox} values. However, we show in the Appendix that in certain circumstances and in the presence of a substantial non-random censoring, an assumption commonly made in survival analysis can lead to misleading results. The second technique, "stacking", has not had any widespread usage in such studies of QSOs. This alternate approach serves as a useful check on the results of survival analysis for the estimation of some ensemble X-ray parameters; however, it does not serve as an estimator of distribution functions.

a) Survival Analysis

Survival analysis was introduced into widespread astronomical use for precisely the current sort of application: Avni *et al.* (1980) developed a technique ("detections and bounds") for incorporating information contained in lower limits, primarily with the intention of investigating the distribution function of α_{ox} for the famous QSOs which were *Einstein* targets. Pfleiderer and Krommidas (1982) reformulated this technique for studies of extragalactic radio sources, using an information theory approach. More recently, it has been realized that the "detections and bounds" method is an independent redevelopment of a statistical approach known as survival analysis which was already in common use in the fields of epidemiology, actuarial science, and industrial reliability (Feigelson and Nelson 1985, Schmitt 1985, and references therein). These latter references also provide an excellent introduction to the field with an emphasis on astronomical applications.

In the current application, there are objects detected in X-rays for which α_{ox} is known, and lower limits on α_{ox} for other objects. A convenient, non-parametric way to estimate the distribution of a random variable (*e.g.*, α_{ox}) in the presence of "right" (lower limit)

censoring has been given by Kaplan and Meier (1958), who provide a maximum likelihood derivation. We desire to estimate the distribution function of α_{ox} values for a sample of n QSOs. Let $S(\alpha_{ox})$ be the so-called "survivor function", the probability of finding a QSO with $\alpha > \alpha_{ox}$. Let α_i be the the true value of α_{ox} for the ith QSO, and $\alpha_i^{\rm lim}$ be the corresponding detection limit (this will vary from QSO to QSO). If $\alpha_i \leq \alpha_i^{\rm lim}$, the object is detected in X-rays; otherwise it is only known that $\alpha_i > \alpha_i^{\rm lim}$. Then let $a_i = \min(\alpha_i, \alpha_i^{\rm lim})$ be the measurement of (or limit on) α_{ox} for the ith QSO; for simplicity, assume the measurements are ordered so that $a_1 < a_2 < \ldots < a_i \ldots a_n$. Then the Kaplan-Meier product limit estimator of the survivor function can be shown to be

$$S(\alpha_{ox}) = \Pi \left(1 - \frac{d_i}{n_i}\right), \tag{4}$$

where $n_i(a_i)$ is the number of objects in the sample with measurements (detections or lower limits) $a > a_i$, $d_i(a_i)$ is the number of detections at a_i, and the product is over values of i such that $a_i \leq \alpha_{ox}$. If the largest observation is censored, then Eq. 4 shows that $S(\alpha_{ox})$ is finite as α_{ox} approaches infinity; to avoid such an unphysical result, the largest observation is commonly treated as uncensored, even when it is censored (*e.g.*, Feigelson and Nelson 1985).

The mean value of α_{ox} is estimated from

$$< \alpha_{ox} >= \int_0^\infty \alpha f(\alpha) d\alpha = \int_0^\infty S(\alpha) d\alpha. \tag{5}$$

$$= \sum_{i=1}^{n+1} S(a_i)\,(a_i - a_{i-1}),$$

(Feigelson and Nelson 1985). If a_n is censored, $S(\infty) > 0$, and $< \alpha_{ox} >$ is formally infinite; hence, the usual practice is again to treat a_n as a detection even if censored. In the Appendix, we show that for certain non-random censoring patterns (in particular, in the presence of a sensitivity threshold), this common assumption can lead to misleading

results. However, this potential pitfall has not significantly compromised published results on X-ray emission from QSOs. Analytical estimates of the uncertainties in the mean of the sample and the survival function are also available (Feigelson and Nelson 1985 and references therein).

b) Stacking

Given the sorts of uncertainties noted in the Appendix for survival analysis, it is desirable to have a second technique to check the former results. Caillault and Helfand (1985) have innovatively applied stacking techniques to X-ray images of the Pleiades in order to estimate the mean X-ray luminosity of Pleiades stars. We have applied this technique to our samples C and N.

i) Mean Flux for Complete Samples

In the X-ray image at the location of each optically selected QSO, the total counts (0.5–3.0 keV) in the $3'$ radius region, and the background counts in the $3 - 5'$ annulus are determined. These counts are summed (*i.e., stacked*) for all QSOs in the sample, and the mean flux of the sample is estimated. For a sample of n QSOs with X-ray images of comparable flux sensitivity, this gives the usual $n^{1/2}$ increase in sensitivity over that in a single X-ray image.

Let S_i be the X-ray source counts (0.5–3.0 keV) for the i-th QSO, so that the X-ray flux (0.5–3.0 keV) for the i-th QSO is $F_i = C_i S_i t_i^{-1}$, where t_i is the integration time of the appropriate X-ray image, and C_i is the conversion factor for transforming broadband count rates into broadband fluxes. Let T_i and B_i be, respectively, the total (background plus source) counts on the source and background counts for the *i-th* QSO. Then, it is readily shown (see A85 for details) that the mean X-ray flux for the sample of n QSOs is

just

$$< F > \simeq < C > \frac{\sum S_i}{\sum t_i} = < C > \frac{(T - B)}{t} \tag{6}$$

where T, B, and t are, respectively, the total counts, background counts, and integration time in the *stacked* image. Further, the uncertainty in this mean flux is (again see A85) just

$$\sigma_{<F>} \simeq < C > \frac{(T + B)^{1/2}}{t} \tag{7}$$

In deriving Eq. 7 we have assumed the following: (1) Poisson statistics; (2) weighting by the inverse of the variance; (3) the background count rate from image to image to approximately constant; (4) either that the individual object count rates are small compared to the background count rates, or that the count rates for all QSOs are approximately equal; and (5) that C_i is approximately constant for all QSOs in the sample.

Thus, although the individual S_i's cannot be accurately determined (for low X-ray fluxes) from the single images, the ensemble average flux can be sensitively measured from the stacked image. The ensemble mean X-ray flux is the quantity required for estimating the contribution of a complete sample of QSOs to the XRB; for this application, it is largely irrelevant how the X-ray flux is distributed among the individual objects. We apply the stacking technique to sample C (§ 5) to obtain such an estimate for QSOs to $B \leq 19.5$ and $1.8 \leq z \leq 3.0$. The possible consequences of flux thresholds on the stacking technique are considered in the Appendix.

ii) Stacking and $\alpha_{ox}^{\rm eff}$ for Sample N

Stacking can also be used for sample N to estimate $\alpha_{ox}^{\rm eff}$; and this will again serve as a useful check on the results of survival analysis. Let $r = l_{2\,\rm keV}/l_{2500}$ be the monochromatic luminosity ratio. Then

$$r = \frac{f_{2\,\rm keV}}{f_{2500}} (1 + z)^{\alpha_x - \alpha_o}, \tag{8}$$

where $f_{2\,\mathrm{keV}}$ and f_{2500} are the monochromatic fluxes in erg cm^{-2} s^{-1} Hz^{-1} in the observer's frame at the respective frequencies. Then for a sample of objects like sample N which occupies a narrow region of L_{opt}, z space and which is imaged in X-rays within images of comparable sensitivity, it can be shown that (see A85) the ensemble mean ratio is

$$< r > \simeq \frac{< C > (1+< z >)^{\alpha_x - \alpha_o} \sum S_i}{\sum f^i_{2500}\, t_i} = \frac{< C > (1+< z >)^{\alpha_x - \alpha_o} (T - B)}{\sum f^i_{2500}\, t_i}, \qquad (9)$$

where T and B have the same meaning as above for the stacked image, but where $< C >$ is now a conversion between broadband counts and monochromatic flux. An estimate of the uncertainty in $< r >$ is

$$\sigma_{<r>} \simeq \frac{< C > (1+< z >)^{\alpha_x - \alpha_o} (T + B)^{1/2}}{\sum f^i_{2500}\, t_i}, \qquad (10)$$

neglecting dispersion introduced by optical flux uncertainties, and by using mean values $< z >$ and $< C >$. Then, an estimate of $\alpha^{\mathrm{eff}}_{ox}$ is given by $\alpha^{\mathrm{eff}}_{ox} = -\log(< r >)/2.605$. Note that the numerator in Eq. 9 is proportional to the total number of X-ray counts emitted jointly from all the QSOs in time t, while the denominator is proportional to the total number of optical counts received in the same time. In § 5 we will use this stacking estimate on sample N to check the results of the survival analysis estimate.

V. X-RAY EMISSION FROM HIGH REDSHIFT QSOs, AND THE CONTRIBUTION OF QSOs TO THE DIFFUSE X-RAY BACKGROUND

a) The Contribution of $B \leq 19.5$ QSOs to the XRB

For an optically complete sample with X-ray information available, one can directly estimate the contribution of such QSOs to the XRB merely by estimating the mean X-ray flux of the sample, and in turn multiplying by the surface density of objects in the complete sample (Marshall *et al.* 1984). The details about how that X-ray flux is distributed among

the individual objects and how α_{ox} depends on other parameters is largely irrelevant for such an application. The 37 sample C QSOs in Table 3 are used in this fashion. The current approach, using a complete sample, is to be strongly contrasted with most optical log N-log S estimates of the contribution of QSOs to the XRB. In their Table 2A, Maccacaro, Gioia, and Stocke (1984) list ~ 21 parameters or uncertain assumptions required in using the usual optical log N-log S approach.

The approach used here with an optically complete sample requires only about six such parameters or assumptions: a complete sample is characterized by the redshift range where it is thought to be complete, the completeness magnitude limit, and a surface density to that limit, and of course one must assume a value for α_x (this latter assumption is the primary uncertainty). With only a half-dozen or so parameters or assumptions involved, this approach is at least competitive with the X-ray luminosity function approach emphasized by Maccacaro, Gioia, and Stocke (1984). Faint, optically complete samples imaged to faint X-ray flux levels are potentially powerful estimators of the contribution of QSOs to the XRB.

i) Survival Analysis of Sample "C"

Application of survival analysis to the 37 sample C objects with X-ray information available yields the following estimate for the mean monochromatic flux at 2 keV: $< S_{2\,\mathrm{keV}} >= (1.24 \pm 0.10) \times 10^{-5}\,\mathrm{keV\ cm^{-2}\ s^{-1}\ keV^{-1}}$ (corresponding to $< F(0.5 - 3.0\,\mathrm{keV}) >= 3.97 \times 10^{-14}\,\mathrm{erg\ cm^{-2}\ s^{-1}}$ in the broadband). The fractional contribution of such QSOs to the XRB is then,

$$f(B \leq 19.5, 1.8 \leq z \leq 3.0) = \frac{I^{\mathrm{QSO}}_{2\,\mathrm{keV}}}{I^{\mathrm{back}}_{2\,\mathrm{keV}}} \approx \frac{n < S_{2\,\mathrm{keV}} >}{I^{\mathrm{back}}_{2\,\mathrm{keV}}} = 0.021 \pm 0.004, \qquad (11)$$

where n is the surface density of the high redshift objects derived for the sample C ($3.02 \pm 0.48\ \mathrm{deg^{-2}}$), and $I^{\mathrm{back}}_{2\,\mathrm{keV}} = 5.84\,\mathrm{keV\ cm^{-2}\ s^{-1}\ ster^{-1}}$ is the XRB intensity at 2 keV (Schwartz

1979). The error estimate of Eq. 11 includes both the uncertainty in the mean flux and that due to Poisson fluctuations in the surface density of QSOs.

ii) Contribution to the XRB of Sample C QSOs Using the Stacking Approach

We have also used stacking to estimate the contribution of sample C QSOs to the XRB. In the stacking technique, it is necessary to exclude QSOs for which the detection region is strongly contaminated by a nearby but not physically associated X-ray source (objects $17272+502$, $17274+503$, and $21556-302$). We also must exclude objects imaged in the HRI, since, for instrumental reasons, they have very different (compared with the IPC) values for C_i and $(T_i+B_i)/t_i$ (§ 4; A85); thus, Obj. 11, Obj. 15, Obj. 16, and $14149+251$ are also excluded in the stacking approach.

Application of the stacking method to the remaining 30 class C QSOs yields for the stacked image T=4348 counts, B=3821 counts, t=526137 s, and thus, $S=(T-B)$=527 counts, $\delta S = (T+B)^{1/2} = 90$ counts, $< s >= S/t = 1.00 \times 10^{-3}$ counts s^{-1}. The mean conversion between broadband count rate and fluxes for these objects is $< C >= 4.34 \times 10^{-11}$ erg cm^{-2} s^{-1} per count s^{-1}, which yields

$$< F(0.5-3.0\,\mathrm{keV}) >= 4.34 \times 10^{-14}\,\mathrm{erg\ cm^{-2}\ s^{-1}} \tag{12}$$

or,

$$< S_{2\,\mathrm{keV}} >= (9.4 \pm 1.9) \times 10^{-6}\,\mathrm{keV\ cm^{-2}\ s^{-1}}. \tag{13}$$

Included in Eq. 13 are the expected uncertainties due to the assumption of the constancy of the the terms C_i and $(T_i+B_i)/t_i$. Effectively, this stacked image has a limiting flux of $2.6 < C > B^{1/2}/t = 1.35 \times 10^{-14}$ erg cm^{-2} s^{-1} (0.5–3.0 keV), comparable to the values reached in the most sensitive "Deep Survey" fields of Giacconi *et al.* (1979*b*).

Thus, for the fractional contribution of sample C QSOs to the XRB, the stacking technique yields:

$$f(B \leq 19.5,\ 1.8 \leq z \leq 3.0) = 0.016 \pm 0.004. \tag{14}$$

This value is within 1σ of that found here using survival analysis. Given the very different approaches, it is comforting that these two estimates are in such good agreement. The fractional contribution found here for sample C QSOs is quite small, and results in part from the low surface density of such high redshift objects, but also from the comparatively low value of X-ray emissivities from these objects (see discussion below).

iii) Contribution of all QSOs with $B \leq 19.5$ to the XRB

Sample C is an excellent complementary sample for combination with the BF sample. We have applied survival analysis to the 14 BF QSOs which have $B < 19.5$ and $z < 1.8$ (and with $M_B < -23.0$). We have not used the stacking technique with the BF objects because the actual counts are not published for the non-detections. For this BF subset, we find

$$< S_{2\,\mathrm{keV}} >= (3.4 \pm 1.4) \times 10^{-5}\,\mathrm{keV\ cm^{-2}\ s^{-1}\ keV^{-1}}. \quad (15)$$

Then to $B \leq 19.5$, the contribution to the XRB from QSOs in the range $0 < z \leq 1.8$ is

$$f(B \leq 19.5, 0 < z \leq 1.8) = 0.16 \pm 0.08. \quad (16)$$

Thus, even using the higher survival analysis value (Eq. 11) for the high redshift QSOs and allowing for $\sim 20\%$ incompleteness in sample C, and 11% in the BF sample (Marshall 1983), we estimate the XRB contribution from QSOs to $B \leq 19.5$ and $0 < z \leq 3.0$ to be

$$f(B \leq 19.5, 0 < z \leq 3.0) = 0.20 \pm 0.08. \quad (17)$$

The surface density of very high redshift QSOs ($z > 3.0$) is the subject of a number of recent and ongoing investigations (Koo and Kron 1980, Osmer 1982, Hazard and McMahon 1985, Schmidt, Schneider, and Gunn 1986). Although the situation is far from settled, it seems likely that unless such QSOs have efficiently escaped selection by current methods, such objects probably have surface densities to $B \leq 19.5$ which (conservatively) are no

more than $\sim 20\%$ of the surface density of QSOs in the redshift range $1.8 \leq z \leq 3.0$ for $B \leq 19.5$. It therefore seems quite unlikely that $z > 3.0$, and $B \leq 19.5$ QSOs contribute more than $\sim 0.4\%$ of the XRB. A reasonable estimate for the contribution of all QSOs to $B \leq 19.5$ to the XRB is thus

$$f(B \leq 19.5) = 0.21 \pm 0.08. \tag{18}$$

As noted earlier, there are a number of reasons to believe that the values estimated above for the contribution of $(B \leq 19.5)$ QSOs to the XRB might be more properly regarded as *upper limits*: (1) possible contamination of Sample C by lower redshift (hence lower L_{opt}, lower α_{ox}) QSOs; (2) α_x may be considerably steeper than 0.5; (3) threshold effects in the survival analysis estimates; (4) probable chance positional coincidence between the order of one sample C QSO and an unrelated X-ray source; (5) possibility that the BF surface density for $B < 19.8$, $z < 2.2$ QSOs is abnormally high (see Marano, Zamorani, and Zitelli 1984 for a discussion of this controversial issue); and, (6) $\sim 40\%$ of the total X-ray flux from the $B \leq 19.5$, $z < 1.8$, subsample arises in a single object, BF 222.

Contamination of the sample C by non-QSOs of course would tend to dilute the ensemble average X-ray flux derived for the sample. However, this diluted X-ray flux is then multiplied by an inflated surface density and these two effects should roughly cancel.

b) The Distribution of α_{ox} Values for Sample N QSOs

Avni and Tananbaum (1982, 1986) have empirically found a dependence of $< \alpha_{ox} >$ on L_{opt} and/or z; which dependence is primary is of current controversy and yet is crucial to proper use of the optical log N-log S approach. Using a collection of optically selected QSOs and Seyferts spanning a large range of L_{opt} and z, they find a primary dependence on L_{opt} using linear regression techniques appropriate for censored data:

$$< \alpha_{ox} >= -0.01[r(z) - 0.5] + 0.118[\log l_{2500} - 30.5] + 1.48. \tag{19}$$

where $\tau(z) = z/(1+z)$ is the fractional lookback time (for $q_0 = 0$), and where we have corrected this expression for a recent IPC effective area recalibration. Such a dependence on L_{opt} can imply substantial ($\geq 50\%$) contributions to the XRB (*e.g.*, A85, Marshall *et al.* 1984), and the relationship of Eq. 19 has been given various physical interpretations (Tucker 1983, Netzer 1985). However, Schmidt and Green (1986), in trying to reconcile data from the XBQS with data from the *Einstein* Medium Sensitivity Survey, favor evolution with redshift such that $L_x/L_{opt} \sim (1+z)^{-2}$. They find values of order only 10% for the contribution of QSOs to the XRB. Selection biases that correlate L_{opt} with z have made it difficult to confidently disentangle the effects of l_{2500} and z on $< \alpha_{ox} >$.

Because of such dependences on L_{opt} and/or z, "observable" quantities such as $< \alpha_{ox} >$, $\alpha_{ox}^{\rm eff}$, and the survivor function for α_{ox} values are immediately interpretable only for a sample of QSOs which occupies a narrow region of L_{opt}, z space. Sample N occupies a sufficiently narrow region of L_{opt}, z space that it can be treated as an empirical data point for QSOs with optical luminosity and redshift equal to the means of the sample: ($< \log(l_{2500}) >= 31.44$) and ($< z >= 2.1$).

i) The Survival Analysis of Sample N

For sample N, the survival function, not merely a single parameter such as $< \alpha_{ox} >$ or $\alpha_{ox}^{\rm eff}$, is of interest, and so it will be generally more productive to use survival analysis rather than the stacking technique. Using the Kaplan-Meier product limit method of survival analysis, we have estimated the distribution of α_{ox} values for the sample N QSOs shown in Figure 3. For sample N the survival analysis estimates yield

$$< \alpha_{ox} >= 1.58 \pm 0.03 \quad \text{and} \quad \alpha_{ox}^{\rm eff} = 1.50 \pm 0.03. \tag{20}$$

These high redshift, high L_{opt} QSOs are indeed comparatively weak in their relative X-ray emissivities. For example, the X-ray selected QSOs (*e.g.*, Margon, Downes, and Chanan 1985; Gioia *et al.* 1984) as well as radio bright QSO (*e.g.*, Zamorani *et al.* 1981.

Tananbaum *et al.* 1983) both have $\alpha_{ox}^{\rm eff} \approx 1.3$; the sample N QSOs have a mean $< L_x/L_{opt} >$ ratio that is $\sim 3-4$ times smaller than that for the X-ray selected and radio bright QSOs.

For the mean parameters, $< \log (l_{2500}) >= 31.44$ and $< z >= 2.1$, appropriate for the sample N QSOs, the model of Avni and Tananbaum (Eq. 19) predicts values of $< \alpha_{ox} >= 1.59$, and $\alpha_{ox}^{\rm eff} = 1.47$. Both values in Eq. 20 are within 1σ of these model predictions. Thus, the measurements of $< \alpha_{ox} >$ and $\alpha_{ox}^{\rm eff}$ for sample N strongly confirm the viability of the relationship found by Avni and Tananbaum for the dependence of $< \alpha_{ox} >$ being (primarily) on L_{opt}. Note that the measurements here have made no assumptions about the particular parametric form (or even the existence!) of the dependence of α_{ox} on L_{opt} and/or z. The measured values of α_{ox} and $\alpha_{ox}^{\rm eff}$ are also independent of uncertainties in H_0 and q_0.

In order to investigate the possibility of redshift evolution of α_{ox}, we have compared our α_{ox} data for sample N with that for various subsets of the XBQS. These subsets of the XBQS are chosen to span the same range in L_{opt} as that spanned by sample N, and the different subsets are appropriate for different assumed values for q_0. These XBQS subsets also span narrow redshift ranges, but at a very much lower mean redshift (typically $< z >\sim 0.3-0.4$ rather than $< z >\sim 2$ for sample N). We use the Mantel-Cox and Breslow-Wilcoxian tests (*e.g.*, Feigelson and Nelson 1985) to test the equality of the distribution for sample N with each of the XBQS subsets. The results are shown in Figure 4. For ease of comparison with the XBQS data, here (and only here), we have assumed $\alpha_o = 0.5$. The formal statistical tests confirm what is apparent to the eye: there is little evidence for redshift evolution. Both tests support the hypothesis that sample N and the XBQS subset arise from different parent distributions only at $\leq 35\%$ confidence level for the cases of $q_0 = 0$ and 0.5. The tests performed here are non-parametric, model-independent empirical evidence against redshift evolution of α_{ox}. Thus, our data support models in which the primary dependence of α_{ox} is on L_{opt} rather than redshift. The pri-

mary uncertainty remaining in this conclusion is the previously mentioned possibility of modest contamination of sample N by low z QSOs.

Since the values for $< \alpha_{ox} >$ and $\alpha_{ox}^{\rm eff}$ found here for sample N are in good agreement with the Avni and Tananbaum model of Eq. 19, we have further used their model to correct the observed sample N distribution for the small (but non-zero) spread in L_{opt}. Following Avni and Tananbaum, we determine, for each sample N QSO, the value (or limit) on the quantity (see Eq. 19)

$$\alpha_{ox}^{\rm corr} = \alpha_{ox} - 0.118\,(\log l_{2500} - 31.44). \qquad (21)$$

The survivor function for these "corrected" values of α_{ox} is shown in Figure 5 and, the corrected values of $< \alpha_{ox} >$ and $\alpha_{ox}^{\rm eff}$ are 1.56 ± 0.03 and 1.50 ± 0.03, respectively. As expected, these values are quite similar to those obtained directly from sample N without any corrections, as can be seen by comparison of Figures 3 and 5. Again, we use the Mantel-Cox and Breslow-Wilcoxian tests to compare the corrected and uncorrected α_{ox} distributions for sample N. The hypothesis that these two distributions actually arise from distinct parent distributions is supported only at the $< 45\%$ confidence level.

ii) The Width of the α_{ox} Distribution for Sample N

Franceschini, Gioia, and Maccacaro (1986), Zamorani (1985), and Avni and Tananbaum (1986) have recently emphasized that the intrinsic width of the α_{ox} distribution, $\sigma(\alpha_{ox})$, about the mean relation of Eq. 19 is an important parameter for understanding the X-ray properties of the QSO population. In particular, the large value (~ 0.2) found by Avni and Tananbaum for the standard deviation of the α_{ox} residuals about the mean dependence on L_{opt}, together with an assumed optical luminosity function, leads to some inconsistencies between X-ray and optically selected samples of QSOs. For example, using the optical luminosity function and the α_{ox} distribution for optically selected QSOs, one can predict the X-ray luminosity function. However, this process with a standard devi-

ation of $\sigma(\alpha_{ox}) \approx 0.2$ found by Avni and Tananbaum (1982) overpredicts by a factor of $\sim 2-3$ (Franceschini, Gioia, and Maccacaro 1986; Avni and Tananbaum 1986) the number of X-ray sources that should have been found in the X-ray selected Medium Sensitivity Survey (Gioia *et al.* 1984) sample. Indeed, the desire to resolve such a discrepancy was a primary motivation for the Schmidt and Green (1986) model of α_{ox} redshift evolution.

Franceschini, Gioia and Maccacaro (1986) suggest that an intrinsic value of $\sigma(\alpha_{ox}) \sim 0.14$ could resolve the apparent discrepancy, and suggest a number of possible external effects that might account for the broadening of the intrinsic distribution, *e.g.*, optical and X-ray variability. In fact, for sample N, we find an observed value of $\sigma(\alpha_{ox}) \sim 0.14$. For the corrected distribution, the standard deviation about the mean dependence of Eq. 19 is $\sigma(\alpha_{ox}^{\rm corr}) = 0.12$.

Superficially, these small standard deviations found for sample N appear quite interesting. However, in the Appendix we show that survival analysis threshold effects can produce an artificial truncation of the distribution which spuriously narrows and skews the survival analysis estimated distribution. It is really the width of the low side of the α_{ox} distribution which is most relevant; the contribution to the standard deviation for α_{ox} less than $< \alpha_{ox} >$ is 0.13 and 0.11, for, respectively, sample N and the corrected sample N. Thus, if the true α_{ox} distribution is approximately Gaussian, the standard deviation in the actual sample N distribution is again likely to be ~ 0.2, in agreement with that found by Avni and Tananbaum. Otherwise, the actual distribution must be quite skewed toward low α_{ox} values.

iii) Stacking Estimate of $\alpha_{ox}^{\rm eff}$ for Sample N

We also have employed the stacking technique to estimate $\alpha_{ox}^{\rm eff}$ for sample N. As with sample C, there are a number of objects not suitable for inclusion in the stacking process: the appropriate data for the 10 QSOs from Kriss and Canizares are not published: six objects are in HRI fields (00151+160, 12275+024, 14149+251, 15090-092, Obj. 11, and

Obj. 15); five are severely contaminated by strong, nearby, but unrelated X-ray sources (03061+169, 11143+184, 17274+503, 17272+502, 21556-302); and two are excluded because they are not imaged to comparable limiting X-ray flux sensitivities (15100-089 and 17252+499). Application of stacking to the remaining 55 suitable sample N QSOs yields

$$\alpha_{ox}^{\rm eff} = 1.53 \pm 0.02. \tag{22}$$

This value is within $\sim 1\sigma$ of the survival analysis estimate for sample N QSOs.

c) The Contribution of QSOs to XRB

Using an optical log N-log S curve, and the α_{ox} dependence on L_{opt} confirmed by our data, one can, in principle, now estimate the contribution of all QSOs to the XRB. However, this involves the introduction of the lengthy list of uncertain assumptions and parameters noted above: note that none of the preceeding results rely on this uncertain approach. Nevertheless, we can at least ask what sorts of contributions are consistent with these data.

For this exercise, we use the optical log N-log S curve of Setti (1984), which he derived using the following QSO samples: the BQS ($B \leq 16.0$, and $z < 2.2$): the "BFG" sample of Braccesi, Formiggini, and Gandolfi (1970) (a color selected sample to $B < 18.3$, and $z < 2.2$); the BF ($B < 19.8$, and $z < 2.2$); the Kron and Chiu (1981) proper motion selected sample ($B \approx 21.1$), and the two-color selected sample of Koo and Kron (1982) ($B \approx 22.6$). In deriving this curve, Setti applied incompleteness corrections by, for example, also using data on high redshift QSOs from slitless spectroscopy surveys, to obtain the following curve for QSOs of *all* absolute magnitudes:

$$\log N(< B) \approx 1.58 + 0.91(B - 20) \quad \text{for} \quad B \leq 20.1 \tag{23}$$

$$\log N(< B) \approx 1.67 + 0.21(B - 20) \quad \text{for} \quad B > 20.1$$

where $N(< B)$ is QSO surface density (counts deg^{-2}). We have made the (uncertain) assumption of a sharp break at $B = 20.1$; a smoother function is a less conservative assumption in this context. Although derived using only counts to $B \sim 22.6$, this model also agrees well with a variety of more recent work (Hamilton 1984, Boyle *et al.* 1985, Borra and Lepage 1986), some of which extends to even fainter magnitudes.

The combined X-ray intensity from all QSOs with magnitudes in the range $B_{\rm min}$ to $B_{\rm max}$, in units of erg cm^{-2} s^{-1} Hz^{-1} ster^{-1}, can be expressed (Zamorani *et al.* 1981) as:

$$I_{2\,\rm keV}^{\rm QSO} = \left(\frac{2500}{4410}\right)^{\alpha_o} (1+z_{\rm eff})^{\alpha_o-\alpha_x} \int_{B_{\rm min}}^{B_{\rm max}} 10^{-0.4B} 10^{-19.380} 10^{-2.605\alpha_{ox}^{\rm eff}} \frac{dN}{dB} dB, \qquad (24)$$

where $z_{\rm eff}$ is the redshift of a typical QSO contributing to the XRB. Here, we define a QSO to have $M_B \leq -23.0$. Then $B_{\rm max}$ is approximately set by the constraint that $M_B(B_{\rm max}, z_{\rm eff}) \leq -23.0$. This latter constraint is equivalent to assuming that all QSOs are at the same redshift $z = z_{\rm eff}$. We take $B_{\rm min} = 16.0$, since brighter QSOs are so rare that their contribution to the XRB will be entirely negligible.

By analogy with the Avni and Tananbaum model of Eq. 19, we presume that $\alpha_{ox}^{\rm eff}$ depends on L_{opt} such that,

$$\alpha_{ox}^{\rm eff} = \alpha_{ox}^{\rm eff}(31.44) + 0.118(\log l_{2500} - 31.44), \qquad (25)$$

where $\alpha_{ox}^{\rm eff}(31.44) = 1.50$ is the value found here for sample N QSOs with $< \log(l_{2500}) >= 31.44$ and $< z >= 2.1$. Then combining Eqs. 23 (extrapolated to as faint as $B \sim 26$), 24, and 25 yields the results in Table 4.

As noted above, the entries in the Table are calculated assuming all QSOs to be at $z_{\rm eff}$. Then, in principle, the actual QSO contribution to the XRB is found by multiplying the Table entries by the fraction all QSOs, as a function of B, that are actually at $z = z_{\rm eff}$, and summing over the rows and columns. Unfortunately, especially at very faint magnitudes, these fractions are not well known; approximately, however, the BF sample, sample C,

and the very faint sample of Koo (1986), suggest that $z_{\rm eff} < 2.5$ to $B \leq 22.6$. Thus, QSO contributions as large as $\sim$ 70% are consistent with these data. The additional contributions of lower luminosity active galaxies and clusters of galaxies might readily account for the remaining $\sim$ 30% of the XRB (Fabian 1981, Schmidt and Green 1986).

Also note from Table 4 that whatever the absolute fraction of the XRB due to QSOs, roughly *half the contribution from QSOs is likely to arise from apparent magnitudes brighter than* $B \sim 20$. *Such QSOs are the sort directly studied in X-rays in the BF sample (Marshall et al. 1984) for* $z < 2.2$, *and in this report for* $z \geq 1.8$. Qualitatively, we also infer the following from Table 4. If QSOs are the dominant contributors to the XRB, the typical contributor is probably a low to moderate optical luminosity QSO (apparent magnitude near the turnover in surface density counts at $B \sim 20$) and at a redshift of $z \sim 1-2$. High redshift QSOs apparently are too scarce, and have too low L_x/L_{opt} ratios, to contribute substantially, while QSOs at $z < 0.5$ are simply too rare to make a substantial contribution.

VI. SUMMARY

We have presented sensitive X-ray information for $\sim$ 90 previously uncataloged QSOs in the redshift range $1.8 \leq z \leq 3$. Even with the longest existing *Einstein Observatory* X-ray exposures, only 25% of these objects are positively detected in X-rays. Among our primary conclusions are the following.

(a) For $B < 19.5$ and $1.8 \leq z \leq 3.0$, our sample C data imply that the fractional contribution of such QSOs to the XRB is less than 3%.

(b) Combining the results for sample C with X-ray data for the BF sample (Marshall 1983), we estimate that the contribution of all QSOs brighter than $B = 19.5$ to the XRB is 21 ± 8%. This estimate, as well as that of point (a), relies only on data from complete samples, and therefore is not subject to the majority of uncertain assumptions, parameters, and extrapolations which are usually required in such an application. The

major uncertainty in these estimates is the value assumed for the X-ray spectral slope; we conservatively (if the estimates above are regarded as upper limits) adopt $\alpha_x = 0.5$.

(c) Because of their apparent dependence on optical luminosity and/or redshift, the parameters $< \alpha_{ox} >$ and $\alpha_{ox}^{\rm eff}$, as well as the distribution of α_{ox} values, are directly interpretable, model independent quantities only if measured in a narrow region of $L_{opt}.z$ space. Our measurements for sample N (which is, by construction, such a "narrow" sample) yield $< \alpha_{ox} >= 1.58$, and $\alpha_{ox}^{\rm eff} = 1.50$, for QSOs with $< \log(l_{2500}) >= 31.44$ ($M_B = -27.5$) and $< z >= 2.1$. These values agree well with the predictions of Avni and Tananbaum (1982, 1986) for dependence of $< \alpha_{ox} >$ on (primarily) optical luminosity. This conclusion, plus our model-independent, non-parametric, empirical comparison of the X-ray data of sample N with that of the recently published "XBQS", do not provide support for the recent suggestion by Schmidt and Green (1986) that the primary dependence of α_{ox} is on z.

(d) The width of the α_{ox} distribution for sample N, $\sigma(\alpha_{ox}) = 0.12 - 0.14$, is smaller than that found by Avni and Tananbaum (1982) for a more heterogenous sample. Although this smaller width potentially could resolve some conflicts between inferences derived from X-ray versus optically selected QSOs, a discrepancy which in part has motivated Schmidt and Green (1986) to suggest reconsideration of the form of X-ray evolution of QSOs, it is likely that α_{ox} threshold effects in survival analysis are artificially narrowing the width of the distribution. The half-width of the distribution below $< \alpha_{ox} >$ is of order 0.1 for sample N, and thus, unless the actual distribution is quite skew, its true full width is probably also $\sigma(\alpha_{ox}) \sim 0.2$, in agreement with the Avni and Tananbaum value.

(e) If we adopt recent QSO surface density counts and the hypothesis of an $< \alpha_{ox} >$ dependence on L_{opt}, we find that QSOs are capable of making the dominant contribution to the XRB at soft energies. Contributions as large as 70% are consistent with

these data, with the typical contributor a moderate redshift ($z \sim 1 - 2$) QSO with $B \sim 19 - 21$. Considerable uncertainty is introduced into this analysis because of the poorly known distribution of X-ray spectral indices of QSOs. However, $\sim 50\%$ of the QSO contribution (regardless of whether or not it is the dominant one) comes from QSOs brighter than $B \sim 20$.

We are indebted to the staffs at the Harvard-Smithsonian Center for Astrophysics, especially Drs. H. Tananbaum and F. Seward, and at KPNO, CTIO, and the CFHT for their aid in obtaining and reducing the data described here, and to a long list of *Einstein Observatory* guest observers who permitted us to examine portions of their data prior to public release. Dr. D. Helfand initially suggested the application of the stacking analysis to our problem. This work has been supported in part by NASA Grant NSG8-433; the first author also gratefully acknowledges the financial support of the ARCS Foundation.

APPENDIX

In many astronomical applications, the presence of detection thresholds results in a quite non-random distribution of the values of the non-detected quantities. We now show by Monte Carlo simulations that such "threshold" effects and an assumption commonly made in survival analysis can produce some very misleading results. Note that thresholds in α_{ox} units can correspond to joint thresholds in optical and X-ray flux sensitivities.

Using a Gaussian random number generator, we generated a synthetic sample of 100 objects which resulted in a distribution with $< \alpha_{ox} >= 1.55$, $\sigma = 0.2$, and $\alpha_{ox}^{\rm eff} = 1.45$ (A85); these values are similar to those found for sample N. The Gaussian form is *not* intended to necessarily represent the actual distribution, but is merely used as a convenient computational form.

First, consider this distribution to be an idealized sample N distribution; in particular, suppose it to be the α_{ox} distribution of 100 QSOs, all of the same L_{opt} and z, and with all

objects imaged in X-rays to the same X-ray flux threshold. For this idealized sample, the X-ray flux limit directly translates into a uniform lower limit on α_{ox} for the non-detections in the sample. We impose this uniform α_{ox} threshold on the idealized distribution, and subject the resulting data to conventional survival analysis to determine $< \alpha_{ox} >$ and $\alpha_{ox}^{\rm eff}$. Finally, we repeat this process for various limiting thresholds. Throughout, we follow the usual practice of treating the highest α_{ox} observation (limit or detection) as though it were uncensored, an assumption shown below to be poor in certain circumstances.

The results of this Monte Carlo simulation are shown in Table A1. The mean α_{ox} value estimated from survival analysis is in quite serious disagreement with the true value for this extreme censoring (threshold) pattern, even when the threshold is sensitive enough to detect $\sim 50\%$ of the objects. The $\alpha_{ox}^{\rm eff}$ estimated from survival analysis is somewhat more reliable, due to its heavy weighting of X-ray bright objects. The systematic underestimate evident in Table A1 can be understood as follows. Again following common practice, we have assumed that the survivor function $S(\alpha_{ox})$ goes to zero at the highest observation (censored or uncensored). That is, the non-parametric survival analysis artificially truncates the distribution; without some prior knowledge of the true distribution function, this is the best it can do.

Note further from Table A1 that such threshold censoring can change the apparent relation between α_{ox} and $\alpha_{ox}^{\rm eff}$, and that the survival analysis error estimates are extremely small (and misleading!) in the presence of significant threshold censoring. This latter point is also readily understood in terms of the premature truncation of the estimated distribution: for α_{ox} thresholds less than $< \alpha_{ox} >$, there are very few objects in the parent distribution with α_{ox} much below the threshold, and of course none (due to truncation) above that threshold, so that in the survival analysis *estimated* distribution, most objects fall close to the threshold. Thus the apparent width of the distribution is underestimated, and the distribution is artificially skewed toward low α_{ox} values.

If a reliable guess cannot be made for the α_{ox} value at which the true distribution has $S(\alpha_{ox}) = 0$, then the uncertainty in $< \alpha_{ox} >$ in the positive direction becomes arbitrarily large in the presence of significant threshold censoring (Avni *et al.* 1980). Then, (see Table A1), in the presence of significant threshold censoring, it is more appropriate to consider survival analysis parameter estimates as lower limits on $< \alpha_{ox} >$ and $\alpha_{ox}^{\rm eff}$.

Now we suppose instead that there are two idealized N-like QSO samples. Further, suppose that one sample, sample A, consists of objects at optical luminosity l_{2500}^a and with redshift z, and the second sample, sample B, consists of objects with optical luminosity l_{2500}^b and also at redshift z (assume that $l_{2500}^a > l_{2500}^b$); and suppose that both samples A and B have the same Gaussian parent distribution of α_{ox} values as that described in the preceeding few paragraphs. By construction, we have assumed no dependence of α_{ox} on L_{opt}. Now we apply a uniform X-ray flux threshold to both samples; since sample A is a collection of more optically luminous objects, it has a more sensitive α_{ox} threshold than sample B, *i.e.*, $\left(\alpha_{ox}^{\rm lim}\right)_A > \left(\alpha_{ox}^{\rm lim}\right)_B$. Conceptually, the results of Table A1 also apply to the latter hypothetical situation; it is seen that the standard survival analysis assumption leads to the clearly mistaken conclusion that the $< L_x/L_{opt} >$ ratio is higher in the lower optical luminosity sample B, than in the higher optical luminosity sample A. For a given redshift, only the optically (and hence X-ray) more luminous objects are detectable at sufficiently high α_{ox} values that the shape of the actual distribution function is well sampled.

Qualitatively, such spurious threshold effects could mimic the sort of dependence of α_{ox} on L_{opt} given physical interpretation by, for example, Tucker (1983) and Netzer (1985). In practice, this sort of threshold effect competes against observational selection: most high L_{opt} QSOs are also at high redshift, and apparently faint in the optical. This latter selection effect tends to make the α_{ox} threshold for high L_{opt} objects systematically smaller than for lower redshift objects. Thus, one must consider the censoring *pattern* to assess the potential influence of threshold effects. We have done this (see A85) for the data analyzed

by Avni and Tananbaum (1982), and see no evidence that the dependence of α_{ox} on L_{opt} which they find results spuriously from the aforementioned threshold effect. Note also that the above sort of sharp cutoff threshold pattern arises naturally in other types of samples in addition to those like sample N (see A85).

Finally, we note that an assumption fundamental to survival analysis is that detections and non-detections arise from the same parent population. This seems reasonable in X-ray studies of QSOs, since substantial fractions (*e.g.*, 50% in the BF and Kriss and Canizares samples, and $\geq$ 80% in the XBQS) of optically selected QSOs are in fact X-ray sources. However, that this assumption has been made must be carefully kept in mind when using survival analysis. For example, were there two distinct populations of QSOs – one X-ray loud and the other X-ray quiet – survival analysis could lead to extremely erroneous conclusions about the distribution of X-ray properties of all QSOs, if it were assumed that X-ray quiet and X-ray loud QSOs alike came from the same parent distribution of X-ray sources: see A85 for a specific numerical example. Avni and Tananbaum (1986) have argued (in a somewhat distribution dependent fashion) that any population of X-ray quiet QSOs is a small ($< 10\%$) fraction of the entire QSO population.

In summary, the effects discussed here, while potentially important in survival analysis, do not appear to have materially affected published results on the XRB.

We have also performed Monte Carlo simulations to assess the influence of X-ray threshold effects on stacking. The model here simulates 100 QSOs, each imaged in X-rays for t_i seconds (all t_i's are assumed equal). In imitation of sample N, the QSOs are assumed to all have $z = 2.1$ and $\log(l_{2500}) = 31.44$; α_{ox} values are again distributed according to the Gaussian distribution used in the earlier Monte Carlo simulation. The ensemble mean IPC counting rate for this synthetic sample would be $< s >= 1.66 \pm 0.096 \times 10^{-3}$ counts s^{-1} in the 0.5-3.0 keV band. For each QSO/image, noise is introduced into the individual S_i's, B_i's, and T_i's. Then the 100 noise-added images are stacked and the ensemble values

of T and B for the stacked image are determined as described above. Finally, this whole process is repeated for different assumed t_i's (*i.e.*, different count rate thresholds) yielding the results of Table A2; the detection fraction listed there is the number of objects that would have been accepted as X-ray detections under guidelines given in § 3. The results are quite encouraging: even in the presence of substantial non-random censoring, stacking apparently is not strongly affected by threshold effects. Compare Table A2 for stacking. with Table A1 for survival analysis, and note that an approximate conversion between an α_{ox} threshold and an integration time threshold can be inferred by comparing the "detection fraction" columns in the two tables.

Table 1. The Complete QSO Sample "C" (B$\leq$ 19.5, 1.8 $\leq z <$ 3.0)

Object[a]	α (1950)	δ (1950)	B	log (l_{2500})	z[b]
08366+654	$08^h36^m37.5^s$	+65°24′01″	19.0	31.57	1.9
08388+131	08 38 48.4	+13 10 00	19.1	31.53	1.88
08388+133	08 38 50.5	+13 19 42	19.0	31.52	1.80
08500+283	08 50 03.6	+28 18 32	19.3	32.11	2.90
09038+167	09 03 52.6	+16 46 15	18.2	32.14	2.4
09379+121	09 37 56.8	+12 09 33	19.0	31.98	2.7[c]
09388+117	09 38 50.8	+11 42 54	18.6	31.87	2.2
09392+121	09 39 14.5	+12 07 24	19.0	31.46	1.80
11131+183	11 13 08.4	+18 21 18	18.6	31.83	2.20
11156+180	11 15 33.3	+18 02 39	18.1	31.85	1.90[c]
12071+398[d]	12 07 11.6	+39 53 24	19.4	31.61	2.33[c]
12076+399	12 07 38.6	+39 56 17	17.5	32.39	2.4
12302+120	12 30 11.0	+12 02 59	19.1	31.45	1.90
12336+264	12 33 28.7	+26 29 54	19.1	31.75	2.40
12354+264[d]	12 35 25.8	+26 27 30	19.4	31.68	2.5
14149+251	14 14 59.5	+25 06 02	18.7	31.63	1.87
14151+254	14 15 08.3	+25 28 45	19.3	31.64	2.31
15181+201	15 18 07.6	+20 07 50	19.2	31.62	2.1
16017+184[d]	16 01 47.0	+18 25 34	19.1	31.51	1.94[c]
17272+502	17 27 12.5	+50 15 07	19.1	31.67	2.1
17272+499	17 27 17.0	+49 56 41	19.3	31.44	1.9
17274+503	17 27 28.1	+50 21 03	19.2	31.66	2.2
20382-012	20 38 16.6	-01 16 21	19.1	32.21	2.9
21342-149	21 34 13.1	-14 55 56	18.3	32.00	2.20

21357-147	21 35 45.7	-14 45 10	19.3	31.57	2.1
21556-302	21 55 40.4	-30 14 27	18.9	31.75	2.20
21570-302	21 57 05.9	-30 14 52	18.4	31.77	1.9
Obj. 5			18.3	31.91	1.96[c]
Obj. 6			19.3	31.67	2.20
Obj. 7			19.2	31.66	2.2
Obj. 8			19.1	32.23	3.00
Obj. 10			19.3	31.53	2.06
Obj. 11			19.1	31.47	1.90
Obj. 12			19.2	31.41	1.90
Obj. 15			19.1	31.60	2.0
Obj. 16			18.2	32.32	2.7
Obj. 17			19.0	31.93	2.6
Obj. 19			19.4	31.63	2.10
Obj. 21			19.4	31.57	2.10

[a] The nomenclature "Obj." is used here and in subsequent tables to honor the proprietary data rights of other observers who generously loaned to us certain fields for this investigation.

[b] Redshifts here and in Table 2 are based on identification of strongest feature as Lα: when more than a single line on the grism/grens plate is detected at a consistent redshift (usually C IV), two decimal places are listed for the redshift (although redshift is still uncertain to ~ 0.1 in z).

[c] Slit spectrum confirms redshift.

[d] Previously cataloged objects (see references in Véron-Cetty and Véron 1985): 12071 + 398 = 1207 + 39W 3, 12354 + 264 = Wee 73, 16017 + 184 = 1601 + 184.

Table 2. The "Narrow" QSO Sample "N"

$(31.0 \leq \log\,(l_{2500}) \leq 32.0,\ 1.8 \leq z \leq 2.5)$

Object	α (1950)	δ (1950)	B	log (l_{2500})	z
00151 + 160	$00^h15^m09.9^s$	+16°03′13″	19.9	31.33	2.20
00159 + 155	00 15 54.8	+15 35 48	20.6	31.07	2.30
01121 − 014	01 12 06.6	−01 26 45	20.3	31.17	2.20
0130 − 404[a]	01 30 45.9	−40 25 49	19.1	31.69	2.16
0130 − 406[a]	01 30 50.7	−40 38 13	18.9	31.88	2.39
0131 − 405[a]	01 31 09.0	−40 35 44	20.4	31.21	2.25
0131 − 402[a]	01 31 36.6	−40 17 56	20.2	31.20	2.11
0131 − 409[a]	01 31 40.0	−40 54 23	19.7	31.55	2.36
0132 − 403[a]	01 32 09.6	−40 18 08	19.4	31.58	2.18
0132 − 408[a]	01 32 20.8	−40 48 26	20.7	31.23	2.46
0132 − 406[a]	01 32 22.2	−40 37 18	19.4	31.56	2.15
02031 + 151	02 03 07.3	+15 09 07	20.3	31.10	2.00
02031 + 152	02 03 08.4	+15 17 04	19.7	31.50	2.38
02036 + 150	02 03 38.4	+15 01 05	19.9	31.32	2.10
02057 + 150	02 05 44.8	+15 00 41	20.5	31.20	2.40
03057 + 172	03 05 45.9	+17 12 12	20.4	31.27	2.40
03061 + 169	03 06 06.7	+16 54 23	20.3	31.21	2.14
03074 + 172	03 07 28.9	+17 16 37	19.2	31.66	2.28
08366 + 654[b]	08 36 37.5	+65 24 01	19.0	31.57	1.9
08388 + 131[b]	08 38 48.4	+13 10 00	19.1	31.53	1.88
08388 + 133[b]	08 38 50.5	+13 19 42	19.0	31.52	1.80
09382 + 117	09 38 13.9	+11 45 32	19.9	31.37	2.30

09382 + 120	09 38 14.7	+12 05 45	19.5	31.42	2.00
09383 + 120	09 38 23.9	+12 05 58	20.2	31.32	2.4
09388 + 117[b]	09 38 50.8	+11 42 54	18.6	31.87	2.2
09392 + 121[b]	09 39 14.5	+12 07 24	19.0	31.46	1.80
09392 + 117	09 39 17.2	+11 46 02	19.8	31.21	1.9
11131 + 183[b]	11 13 08.4	+18 21 18	18.6	31.83	2.20
11136 + 182	11 13 41.9	+18 12 53	19.5	31.29	1.9
11143 + 184	11 14 19.2	+18 28 38	20.3	31.15	2.20
11156 + 180[b]	11 15 33.3	+18 02 39	18.1	31.85	1.90
11147 + 183	11 14 46.6	+18 19 42	19.7	31.21	1.9
12071 + 398[b]	12 07 11.6	+39 53 24	19.4	31.61	2.33
12275 + 024	12 27 35.3	+02 28 47	20.2	31.12	2.0
12292 + 116[c]	12 29 12.4	+11 37 48	19.7	31.14	1.80
12302 + 120[b]	12 30 11.0	+12 02 59	19.1	31.45	1.90
12336 + 264[b]	12 33 28.7	+26 29 54	19.1	31.75	2.40
12354 + 264[b]	12 35 25.8	+26 27 30	19.4	31.68	2.5
14144 + 256	14 14 29.9	+25 36 42	19.6	31.22	1.80
14148 + 252	14 14 49.7	+25 13 34	19.7	31.20	1.83
14149 + 251[b]	14 14 59.5	+25 06 02	18.7	31.63	1.87
14151 + 254[b]	14 15 08.3	+25 28 45	19.3	31.64	2.31
15090 − 092	15 09 03.4	−09 17 09	19.9	31.18	1.9
15100 − 089	15 10 00.5	−08 57 48	20.4	31.17	2.1
15181 + 201[b]	15 18 07.6	+20 07 50	19.2	31.62	2.1
15184 + 202	15 18 25.9	+20 17 33	19.9	31.34	2.10
16016 + 184	16 01 38.3	+18 24 08	20.2	31.24	2.31
16017 + 184[b]	16 01 47.0	+18 25 34	19.1	31.51	1.94
1623 + 269[a]	16 23 25.4	+26 54 41	19.6	31.66	2.44

$1624+269^{a}$	16 24 03.1	+26 57 33	18.3	32.00	2.20
17252 + 499	17 25 14.1	+49 57 46	19.9	31.20	1.90
17257 + 503	17 25 43.4	+50 18 15	20.4	31.15	2.1
17264 + 504	17 26 25.3	+50 28 30	19.9	31.20	1.9
$17272+502^{b}$	17 27 12.5	+50 15 07	19.1	31.67	2.1
$17272+499^{b}$	17 27 17.0	+49 56 41	19.3	31.44	1.9
$17274+503^{b}$	17 27 28.1	+50 21 03	19.2	31.66	2.2
17449 + 206	17 44 59.1	+20 36 05	19.0	31.91	2.41
17465 + 201	17 46 33.3	+20 10 58	19.0	31.64	1.90
20374 − 007	20 37 25.8	−00 44 39	19.9	31.47	2.3
20381 − 011	20 38 10.9	−01 09 10	20.4	31.25	2.26
21189 + 168	21 18 59.9	+16 51 26	19.5	31.64	2.30
21259 − 148	21 25 57.4	−14 51 02	19.9	31.38	2.30
21265 − 150	21 26 34.1	−15 02 39	20.3	31.18	2.1
$21342-149^{b}$	21 34 13.1	−14 55 56	18.3	32.00	2.20
21354 − 145	21 35 27.8	−14 32 11	19.9	31.18	1.90
$21357-147^{b}$	21 35 45.7	−14 45 10	19.3	31.57	2.1
$21416+037^{d}$	21 41 40.5	+03 45 07	20.2	31.05	1.8
21431 + 040	21 43 10.8	+04 03 59	19.2	31.57	2.0
21558 + 034	21 55 51.2	+03 29 33	19.0	31.56	1.9
$21556-302^{b}$	21 55 40.4	−30 14 27	18.9	31.75	2.20
$21570-302^{b}$	21 57 05.9	−30 14 52	18.4	31.77	1.9
Obj. 1			20.4	31.13	2.20
Obj. 2			18.7	31.97	2.5
Obj. 3			20.3	31.20	2.30
Obj. 4			19.1	31.61	2.0
Obj. 5^{b}					

Obj. 6[b]			
Obj. 7[b]			
Obj. 9	20.2	31.18	2.1
Obj. 10[b]			
Obj. 11[b]			
Obj. 12[b]			
Obj. 13	20.1	31.22	2.1
Obj. 14	20.2	31.20	2.2
Obj. 15[b]			
Obj. 18	18.9	31.81	2.0
Obj. 19[b]			
Obj. 20	20.2	31.35	2.3
Obj. 21[b]			

[a] QSOs discovered in previous grism surveys, whose X-ray properties have been studied by Kriss and Canizares (1985): l_{2500} has been recalculated assuming $\alpha_o = 1.0$.

[b] QSO also in Sample C: details in Table 1.

[c] Identical to object U9 of He *et al.* (1984).

[d] Coincident within the positional errors with the 5 GHz radio source MG2144+0358 (Bennett *et al.* 1986).

Table 3. X-Ray Data for Sample C and N QSOs[a]

Object	Significance[b]	$F_{obs} \times 10^{13}$ (erg cm^{-2} s^{-1}, 0.5-3.0 keV)	log ($l_{2\,keV}$)	α_{ox}
00151 + 160	0.7	< 0.688	< 28.24	> 1.19
00159 + 155	0.2	< 0.565	< 27.70	> 1.29
0130 − 404[c]			27.97	1.43
0130 − 406[c]			< 27.62	> 1.64
0131 − 405[c]			< 27.54	> 1.41
0131 − 402[c]			27.77	1.32
0131 − 409[c]			< 27.58	> 1.52
0132 − 403[c]			27.83	1.44
0132 − 408[c]			< 27.56	> 1.41
0132 − 406[c]			< 27.44	> 1.58
02031 + 151	−0.7	< 0.641	< 27.60	> 1.34
02036 + 150	1.3	< 0.633	< 27.65	> 1.41
03061 + 169	2.1	< 0.645	< 27.71	> 1.34
08366 + 654	0.4	< 0.728	< 27.59	> 1.53
08388 + 131	2.1	< 0.766	< 27.60	> 1.51
08388 + 133	1.7	< 0.735	< 27.53	> 1.53
08500 + 283	0.2	< 0.692	< 28.07	> 1.55
09038 + 167	0.0	< 0.882	< 27.95	> 1.61
09379 + 121	−0.2	< 0.601	< 27.91	> 1.56
09382 + 117	−0.1	< 0.670	< 27.77	> 1.38
09382 + 120	1.3	< 0.576	< 27.54	> 1.49
09383 + 120	−0.8	< 0.597	< 27.77	> 1.36

	2.0	47	< 27.73	> 1.59
$09388 + 117$	1.6	< 0.683	< 27.46	> 1.54
$09392 + 121$	2.2	< 0.629	< 27.54	> 1.41
$09392 + 117$	-0.6	< 0.652	< 27.65	> 1.60
$11131 + 183$	-2.0	< 0.593	< 27.54	> 1.44
$11136 + 182$	2.1	< 0.682	< 27.70	> 1.33
$11143 + 184$	1.8	< 0.661	< 27.55	> 1.40
$11147 + 183$	1.9	< 0.692	< 27.61	> 1.63
$11156 + 180$	1.8	< 0.795	< 27.73	> 1.49
$12071 + 398$	0.1	< 0.608	< 27.81	> 1.76
$12076 + 399$	-0.5	< 0.680	< 28.20	> 1.12
$12275 + 034$	2.0	< 2.690	< 27.53	> 1.39
$12292 + 116$	-0.4	< 0.747	< 27.83	> 1.39
$12302 + 120$	1.1	< 1.310	< 27.81	> 1.49
$12354 + 264$	2.1	< 0.599	< 27.41	> 1.46
$14148 + 252$	-0.9	< 0.552	< 29.49	> 0.82
$14149 + 251$	1.6	< 1.160	< 27.86	> 1.45
$14151 + 254$	1.5	< 0.653	< 28.15	> 1.16
$15090 - 092$	0.2	< 2.610	< 28.37	> 1.07
$15100 - 089$	-0.9	< 1.250	< 27.56	> 1.45
$15184 + 202$	2.3	< 0.512	< 27.75	> 1.34
$16016 + 184$	1.5	< 0.625	< 27.51	> 1.54
$16017 + 184$		< 0.578	< 27.63	> 1.55
$1623 + 269^c$			27.50	1.76
$1624 + 269^c$		< 0.594	< 27.50	> 1.42
$17252 + 499$	-2.0	< 0.558	< 27.59	> 1.37
$17257 + 503$	-0.3	< 0.564	< 27.48	> 1.43
$17264 + 504$	1.4			

17272 + 502	< 87.7	< 1.53×10^4	< 30.03	> 0.63
17272 + 499	−1.2	< 0.633	< 27.53	> 1.50
17274 + 503	< 2.1	< 0.521	< 27.61	> 1.55
17465 + 201	0.3	< 0.646	< 28.56	> 1.18
20381 − 011	1.5	< 0.643	< 27.76	> 1.34
20382 − 012	2.1	< 0.561	< 28.00	> 1.62
21259 − 148	1.6	< 0.674	< 27.79	> 1.38
21265 − 150	0.6	< 0.662	< 27.67	> 1.35
21342 − 149	1.3	< 0.710	< 27.75	> 1.63
21354 − 145	1.2	< 0.787	< 27.63	> 1.36
21357 − 147	2.0	< 0.715	< 27.70	> 1.49
21416 + 037	1.2	< 0.658	< 27.52	> 1.36
21431 + 040	−1.6	< 0.836	< 27.72	> 1.48
21558 + 034	0.7	< 0.712	< 27.59	> 1.52
21556 − 302	< 2.1	< 1.130	< 27.94	> 1.46
21570 − 302	1.7	< 1.080	< 27.75	> 1.54
Obj. 1	2.7	0.493	27.59	1.36
Obj. 2	3.0	0.689	27.90	1.56
Obj. 3	6.2	1.280	28.06	1.20
Obj. 4	3.6	0.597	27.59	1.54
Obj. 5	4.8	0.533	27.61	1.65
Obj. 6	2.8	0.422	27.49	1.60
Obj. 7	3.4	0.925	27.86	1.46
Obj. 8	4.4	1.110	28.33	1.50
Obj. 9	2.9	0.685	27.68	1.35
Obj. 10	3.5	0.765	27.69	1.48
Obj. 11	2.8	0.265	27.60	1.48

Obj. 12	3.3	0.876	27.66	1.44
Obj. 13	3.4	0.914	27.79	1.32
Obj. 14	4.5	1.220	27.97	1.24
Obj. 15	2.1	< 0.648	< 28.06	> 1.36
Obj. 16	-0.2	< 0.459	< 28.27	> 1.56
Obj. 17	2.7	0.664	27.92	1.54
Obj. 18	10.1	2.050	28.13	1.41
Obj. 19	2.9	0.693	27.70	1.51
Obj. 20	7.9	2.800	28.41	1.13
Obj. 21	2.7	0.688	27.74	1.48

[a] QSOs in the sample which lie within an optical grism/grens plate, but lie outside the usable area of the X-ray image (*e.g.*, on the "ribs" in the IPC), have incomplete X-ray information and are omitted from the table.

[b] Ratio of source counts/(background counts)$^{1/2}$ in 3′ radius circle.

[c] X-ray data from Kriss and Canizares (1985), but with α_{or} adjusted for the assumption of $\alpha_o = 1.0$.

Table 4. Fractional Contribution of QSOs to the XRB,

Assuming α_{ox} Dependence on L_{opt}

z_{eff} =	0.5	1.0	1.5	2.0	2.5	3.0	3.5
(B_{max}) =	(19.87)	(21.77)	(22.99)	(23.90)	(24.64)	(25.27)	(25.81)
Δ B							
16-17	0.006	0.004		0.003		0.002	
17-18	0.025	0.017		0.012		0.009	
18-19	0.109	0.074		0.049		0.039	
19-20	0.363	0.316		0.212		0.166	
20-21		0.206		0.138		0.108	
21-22		0.106		0.091		0.071	
22-23				0.078		0.061	
23-24				0.060		0.052	
24-25						0.045	
25-26						0.011	
16-B_{max}	0.503	0.722	0.686	0.642	0.600	0.564	0.532
16-19.5	0.293	0.198	0.157	0.132	0.116	0.104	0.095

Table A1. Non-Random Threshold Effects in Survival Analysis

α_{ox}^{thresh}	$< \alpha_{ox} >$	α_{ox}^{eff}	detection fraction
1.3	1.29 ± 0.002 (13.0)	1.29 ± 0.01 (7.2)	.11
1.4	1.38 ± 0.005 (8.2)	$1.37(-.01, +.005)$ (3.6)	.27
1.5	1.44 ± 0.009 (5.0)	$1.41(-0.01, +.02)$ (1.4)	.44
1.6	1.49 ± 0.013 (2.5)	$1.44(-.02, +.01)$ (< 1)	.62
1.7	1.52 ± 0.016 (1.2)	$1.44(-.01, +.02)$ (< 1)	.78
1.8	1.54 ± 0.018 (< 1)	1.45 ± 0.02 (< 1)	.90
1.9	1.54 ± 0.019 (< 1)	1.45 ± 0.02 (< 1)	.93
2.0	1.55 ± 0.020 (< 1)	1.45 ± 0.02 (< 1)	.99
2.1	1.55 ± 0.020 (< 1)	1.45 ± 0.02 (< 1)	1.00

Note: numbers in the rightmost set of parentheses within the second and third columns show the significance (in σ's) of the difference between the survival analysis estimate and the chosen values of $< \alpha_{ox} >= 1.55$ and $\alpha_{ox}^{eff} = 1.45$.

Table A2. Threshold Effects in Stacking

t_i(s)	$< s >$ (10^{-3} counts s^{-1})	detection fraction
20,000	1.634 ± 0.090	0.38
10,000	1.624 ± 0.128	0.27
5,000	1.610 ± 0.179	0.17
1,000	1.551 ± 0.396	0.03

REFERENCES

Anderson, S. F. 1985, Ph. D. thesis, University of Washington ("A85").

Anderson, S. F., and Margon, B. 1983, in "Quasars and Gravitational Lenses", Proc. 24th Liège Int. Ap. Colloq., (Université de Liège), p. 68.

Anderson, S. F., and Margon, B. 1984, in *X-ray and UV Emission from Active Galactic Nuclei*, ed. W. Brinkmann and J. Trümper (Munich: Max Planck Institute), p. 132.

Anderson, S. F., and Margon, B. 1986, in *Quasars, IAU Symposium 119*, ed. G. Swarup and V. K. Kapahi (Dordrecht: Reidel), in press.

Avni, Y., Soltan, A., Tananbaum, H., Zamorani, G. 1980, *Ap. J.*, **238**, 800.

Avni, Y., and Tananbaum, H. 1982, *Ap. J. (Letters)*, **262**, L17.

Avni, Y., and Tananbaum, H. 1986, *Ap. J.*, **305**, 83.

Bennett, C. L., Lawrence, C. R., Burke, B. F., Hewitt, J. N., and Mahoney, J. 1986, *Ap. J. Suppl.*, **61**, 1.

Borra, E. F., and Lepage, R. 1986, *A. J.*, **92**, 203.

Boyle, B. J., Fong, R., Shanks, T., and Clowes, R. G. 1985, *M.N.R.A.S.*, **216**, 623.

Braccesi, A., Formiggini, L., and Gandolfi, E. 1970, *Astr. Ap.*, **5**, 264.

Caillault, J.-P., and Helfand, D. J. 1985, *Ap. J.*, **289**, 279.

Carswell, R. F., and Smith, M. G. 1978, *M.N.R.A.S.*, **185**, 381.

Clowes, R. G. 1981, *M.N.R.A.S.*, **197**, 731.

Crampton, D., Schade, D., and Cowley A. P. 1985, *A. J.*, **90**, 987.

De Zotti, G., Boldt, E. A., Cavaliere, A., Danese, L., Franceschini, A., Marshall, F. E., Swank, J. H., and Szymkowiak, A. E. 1982, *Ap. J.*, **253**, 47.

Elvis, M., and Lawrence, A. 1985, in *Astrophysics of Active Galaxies and Quasi-Stellar Objects*, ed. J. S. Miller (Mill Valley, CA: Univ. Science Books), p. 289.

Elvis, M., Wilkes, J. B., and Tananbaum, H. 1985, *Ap. J.*, **292**, 357.

Fabian, A. C. 1981, *Ann. N. Y. Acad. Sci.*, **375**, 235.

Feigelson, E. D., and Nelson, P. I. 1985, *Ap. J.*, **293**, 192.

Formiggini, L., Zitelli, V., Bonoli, F., and Braccesi, A. 1980, *Astr. Ap. Suppl.*, **39**, 129.

Franceschini, A., Gioia, I. M., and Maccacaro, T. 1986, *Ap. J.*, **301**, 124.

Gaston, B. 1983, *Ap. J.*, **272**, 411.

Giacconi, R., Gursky, H., Paolini, F. R., and Rossi, B. B. 1962, *Phys. Rev. Letters*, **9**, 439.

Giacconi, R., *et al.* 1979*a*, *Ap. J.*, **230**, 540.

Giacconi, R., *et al.* 1979*b*, *Ap. J. (Letters)*, **234**, L1.

Giacconi, R., *et al.* 1981, in *Telescopes for the 1980's*, ed. G. Burbidge and A. Hewitt, (Palo Alto: Annual Reviews), p. 195.

Gioia, I. M., *et al.* 1984, *Ap. J.*, **283**, 486.

Hamilton. D. 1984, in *IAU Colloquium 78, Astronomy with Schmidt-Type Telescopes*, ed. M. Capaccioli (Dordrecht: Reidel), p. 461.

Harnden. Jr., F. R., Fabricant, D. G., Harris, D. E., and Schwartz, J. 1984, "Scientific Specification of the Data Analysis System for the Einstein Observatory (HEAO-2) Imaging Proportional Counter", SAO Special Rep. 393.

Hayman, P. G., Hazard, C., and Sanitt, N. 1979, *M.N.R.A.S.*, **189**, 853.

Hazard, C., and McMahon, R. 1985, *Nature*, **314**, 238.

He, X.-T., Cannon, R. D., Peacock, J. A., Smith. M. G., and Oke, J. B. 1984, *M.N.R.A.S.*, **211**, 443.

Hoag, A. A., and Smith, M. G. 1977, *Ap. J.*, **217**, 362.

Kaplan, E. L., and Meier, P. 1958, *J. Am. Stat. Assoc.*, **53**, 457.

Koo, D. C., and Kron, R. G. 1980, *Pub. A. S. P.*, **92**, 537.

Koo, D. C., and Kron, R. G. 1982, *Astr. Ap.*, **105**, 107.

Koo, D. C. 1986, in *Structure and Evolution of Active Galactic Nuclei*, ed. G. Giuricin, F. Mardirossian, M. Mezzetti, and M. Ramella (Dordrecht: Reidel), p. 317.

Kriss, G. A., and Canizares, C. R. 1982, *Ap. J.*, **261**, 51.

Kriss, G. A., and Canizares, C. R. 1985, *Ap. J.*, **297**, 177.

Kron, R. G., and Chiu, G. L.-T. 1981, *Pub. A. S. P.*, **93**, 397.

Ku, W. H.-M., Helfand, D. J., and Lucy, L. B. 1980, *Nature*, **288**, 323.

Maccacaro, T., Gioia, I. M., and Stocke, J. T. 1984, *Ap. J.*, **283**, 486.

Marano, B., Zamorani, G., and Zitelli, V. 1984, *The Messenger*, **38**, 6.

Margon, B., Downes R. A., and Chanan, G. A. 1985, *Ap. J. Suppl.*, **59**, 1.

Marshall, H. L. 1983, Ph.D. thesis, Harvard Univ.

Marshall, H. L., Avni, Y., Braccesi, A., Huchra, J. P., Tananbaum, H., Zamorani, G., and Zitelli, V. 1984, *Ap. J.*, **283**, 50.

Mushotzky, R. F., Marshall, F. E., Boldt, E. A., Holt, S. S., and Serlemitsos, P. J. 1980, *Ap. J.*, **235**, 377.

Netzer, H. 1985, *M.N.R.A.S.*, **216**, 63.

Osmer, P. S. 1980, *Ap. J. Suppl.*, **42**, 523.

Osmer, P. S. 1982, *Ap. J.*, **253**, 28.

Petre, R., Mushotzky, R. F., Krolik, J. H., and Holt, S. S. 1984, *Ap. J.*, **280**, 499.

Pfleiderer, J., and Krommidas, P. 1982, *M.N.R.A.S.*, **198**, 281.

Reichert, G. A., Mason, K. O., Thorstensen, J. R., and Bowyer, S. 1982, *Ap. J.*, **240**, 347.

Rothschild, R. E., Mushotzky, R. F., Baity, W. A., Gruber, D. E., Matteson, J. L., and Peterson, L. E. 1983, *Ap. J.*, **269**, 423.

Sandage, A., and Katem, B. 1977, *Ap. J.*, **215**, 62.

Schmidt, M. 1968, *Ap. J.*, **151**, 393.

Schmidt, M., and Green, R. F. 1983, *Ap. J.*, **269**, 352.

Schmidt, M., and Green, R. F. 1986, *Ap. J.*, **305**, 68.

Schmidt, M., Schneider, D. P., and Gunn, J. E. 1986, *Ap. J.*, **306**, 411.

Schmitt, J. H. M. M. 1985, *Ap. J.*, **293**, 178.

Schwartz, D. 1979, in "X-ray Astronomy", Proc. IAU/COSPAR Symp., ed. W. A. Baity and L. E. Peterson (eds.), *Adv. Space Exploration*, **3**, (Oxford: Pergamon), p. 453.

Setti, G. 1984, in *X-ray and UV Emission from Active Galactic Nuclei*, ed. W. Brinkmann and J. Trümper (Munich: Max Planck Institute), p. 243.

Setti, G., and Woltjer, L. 1979, *Astr. Ap.*, **76**, L1.

Smith, M. G. 1981, in *Investigating the Universe*, ed. F. P. Kahn, (Dordrecht: Reidel), p. 151.

Smith, M. G. 1982, in *Progress in Cosmology*, ed. A. W. Wolfendale (Dordrecht: Reidel), p. 275.

Sramek, R. A., and Weedman, D. W. 1978, *Ap. J.*, **221**, 468.

Tananbaum, H. *et al.* 1979, *Ap. J. (Letters)*, **234**, L9.

Tananbaum, H., Wardle, J. F. C., Zamorani, G., and Avni, Y. 1983, *Ap. J.*, **268**, 60.

Tananbaum, H., Avni, Y., Green, R. F., Schmidt, M., and Zamorani, G. 1986, *Ap. J.*, **305**, 57.

Tucker, W. H. 1983, *Ap. J.*, **271**, 531.

Vaucher, B., and Weedman, D. W. 1980, *Ap. J.*, **240**, 10.

Véron, P. 1983, in "Quasars and Gravitational Lenses", Proc. 24th Liège Int. Ap. Colloq., (Université de Liège), p. 210.

Véron-Cetty, M.-P., and Véron, P. 1985, "A Catalogue of Quasars and Active Nuclei (2nd Edition)", ESO Scientific Rep. No. 4.

Weedman, D. W. 1985, *Ap. J. Suppl.*, **57**, 523.

Wilkes, B. J. 1986, *M.N.R.A.S.*, **218**, 331.

Worrall, D. M., Mushotzky, R. F., Boldt, E. A., Holt, S. S., and Serlemitsos, P. J. 1979, *Ap. J.*, **232**, 683.

Zamorani, G. *et al.* 1981, *Ap. J.*, **245**, 357.

Zamorani, G. 1985, *Ap. J.*, **299**, 814.

Figure Captions

Figure 1. The distribution of apparent B magnitudes for the grism/grens emission line selected QSOs (mainly at high redshift) discovered on the best quality plate material. Note the decrease at magnitudes fainter than the peak, which we interpret as due to the onset of incompleteness at $B \sim 19.5$.

Figure 2. The reliability of magnitudes estimated from POSS has been tested through measurement of two samples with photometric data. *Triangles*, the spectrophotometrically calibrated QSO sample of Vaucher and Weedman (1980), using those authors' 4500 Å continuum magnitudes; *squares*, the M15 photoelectric sequence of Sandage and Katem (1977).

Figure 3. The survivor function for α_{ox} values of QSOs in sample N ($1.8 \leq z \leq 2.5$, $31.0 \leq log(l_{2500}) \leq 32.0$). This function S($\alpha$) describes the probability that a QSO will have an α_{ox} value in excess of α. *Vertical broken lines*, $\alpha_{ox}^{\rm eff}$ values typical of X-ray selected samples (Gioia *et al.* 1984, Margon, Downes, and Chanan 1985), and the UV-selected sample studied by Marshall *et al.* (1984). Note that many of the QSOs studied here have higher α_{ox} values, and are thus significantly more "X-ray quiet", than those of past work. For our sample, $\alpha_{ox}^{\rm eff} = 1.50 \pm 0.03$.

Figure 4. A comparison of the sample N α_{ox} survivor function (*solid line*) for high redshift QSOs with those of low redshift, XBQS QSOs of comparable L_{opt}. Sample N QSOs ($z = 1.8 - 2.5$) span a range in optical luminosity of $30.8 < log(l_{2500}) < 32.0$ and $30.5 < log(l_{2500}) < 31.6$ for $q_0 = 0$ and 0.5, respectively. This function differs from that shown in Figure 3 because here we assume $\alpha_o = 0.5$ for ease of comparison with the XBQS. *Broken*

line, α_{ox} distribution for the XBQS subset that spans the same L_{opt} range as sample N assuming $q_0 = 0$, and that occupies a similarly narrow, but much lower, redshift range, $z = 0.16 - 0.62$; this first XBQS subset includes 12 objects, of which 10 are detected in X-rays. *Dotted line*, α_{ox} distribution of the XBQS subset in the appropriate L_{opt} range for comparison with sample N, for the case of $q_0 = 0.5$; this subset spans $z = 0.14 - 0.62$, and includes 19 objects, 17 of which are detected in X-rays. A typical error bar for the XBQS distribution is shown in the upper right hand corner. The similarity of the survivor functions for sample N at $< z >= 2.1$ and the XBQS subsets at $< z >= 0.3 - 0.4$ (see text for statistics) argues against substantial redshift evolution of α_{ox}.

Figure 5. Survivor function for α_{ox} values of sample N, with corrections applied for the correlation of α_{ox} with optical luminosity. As described in the text, the corrections are sufficiently small that this distribution is virtually indistinguishable from that of Figure 3.

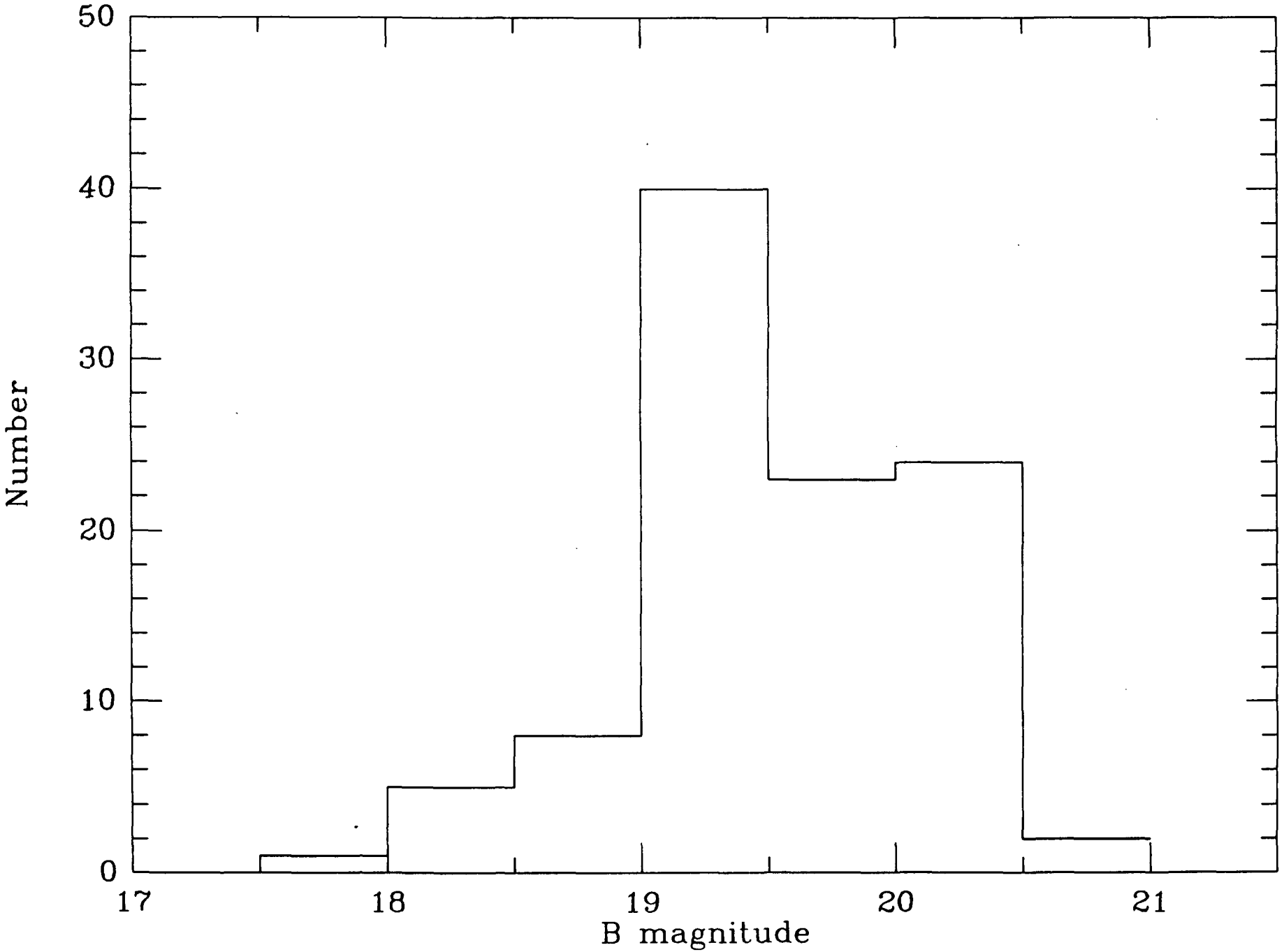

Figure 1

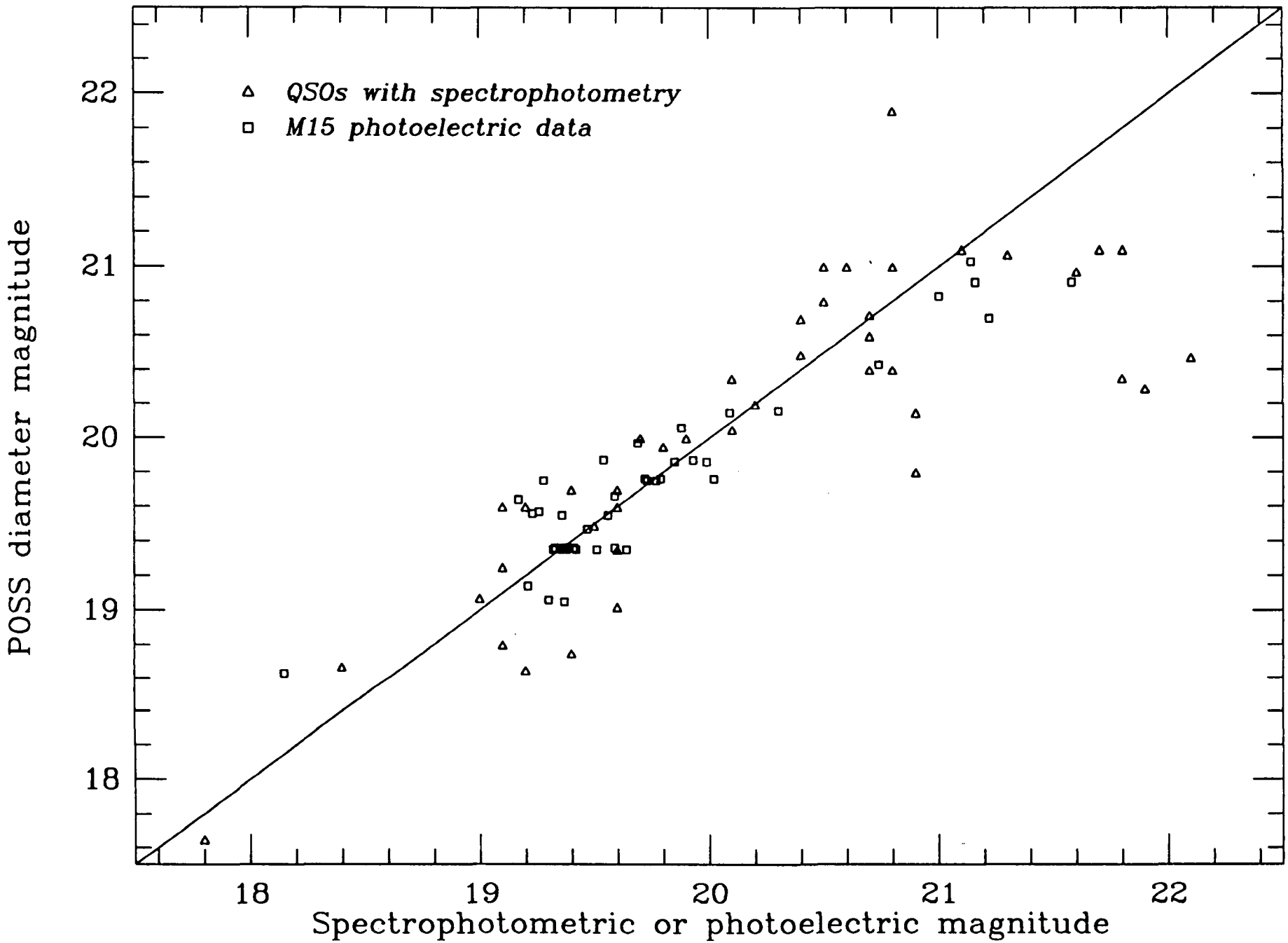
QSOs with spectrophotometry
M15 photoelectric data
POSS diameter magnitude
Spectrophotometric or photoelectric magnitude
18
19
20
21
22

Figure 2

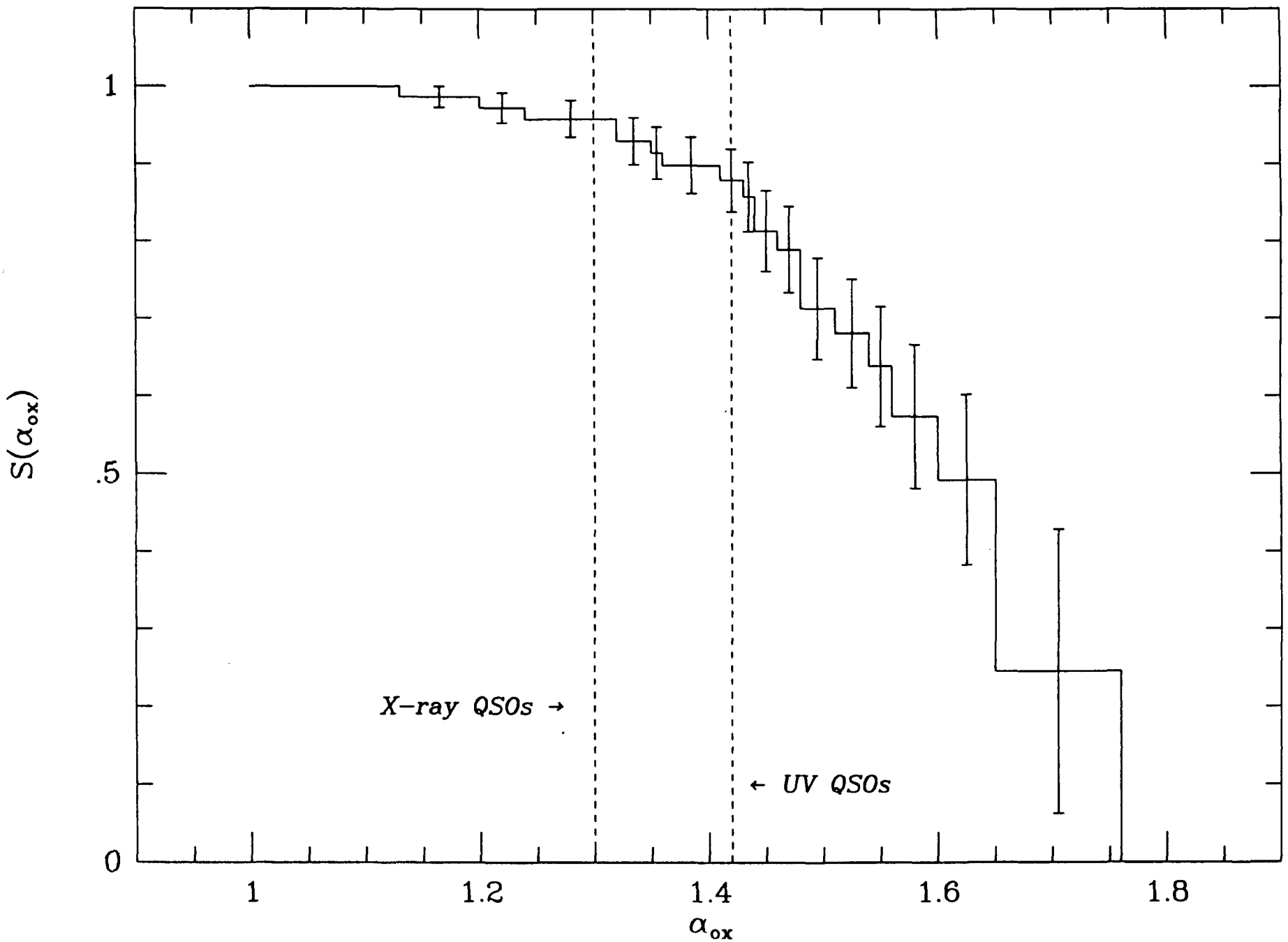

Figure 3

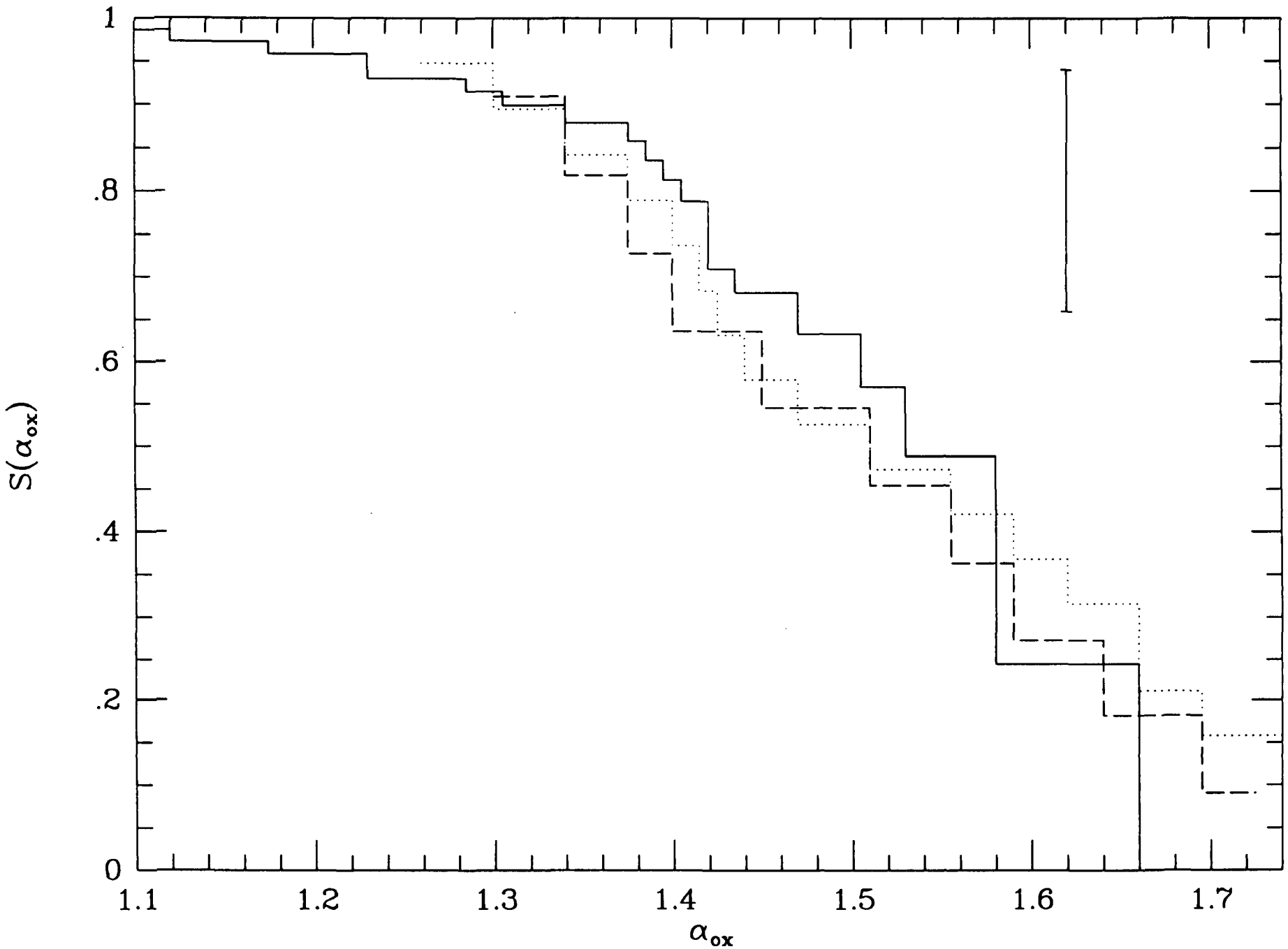

Figure 4

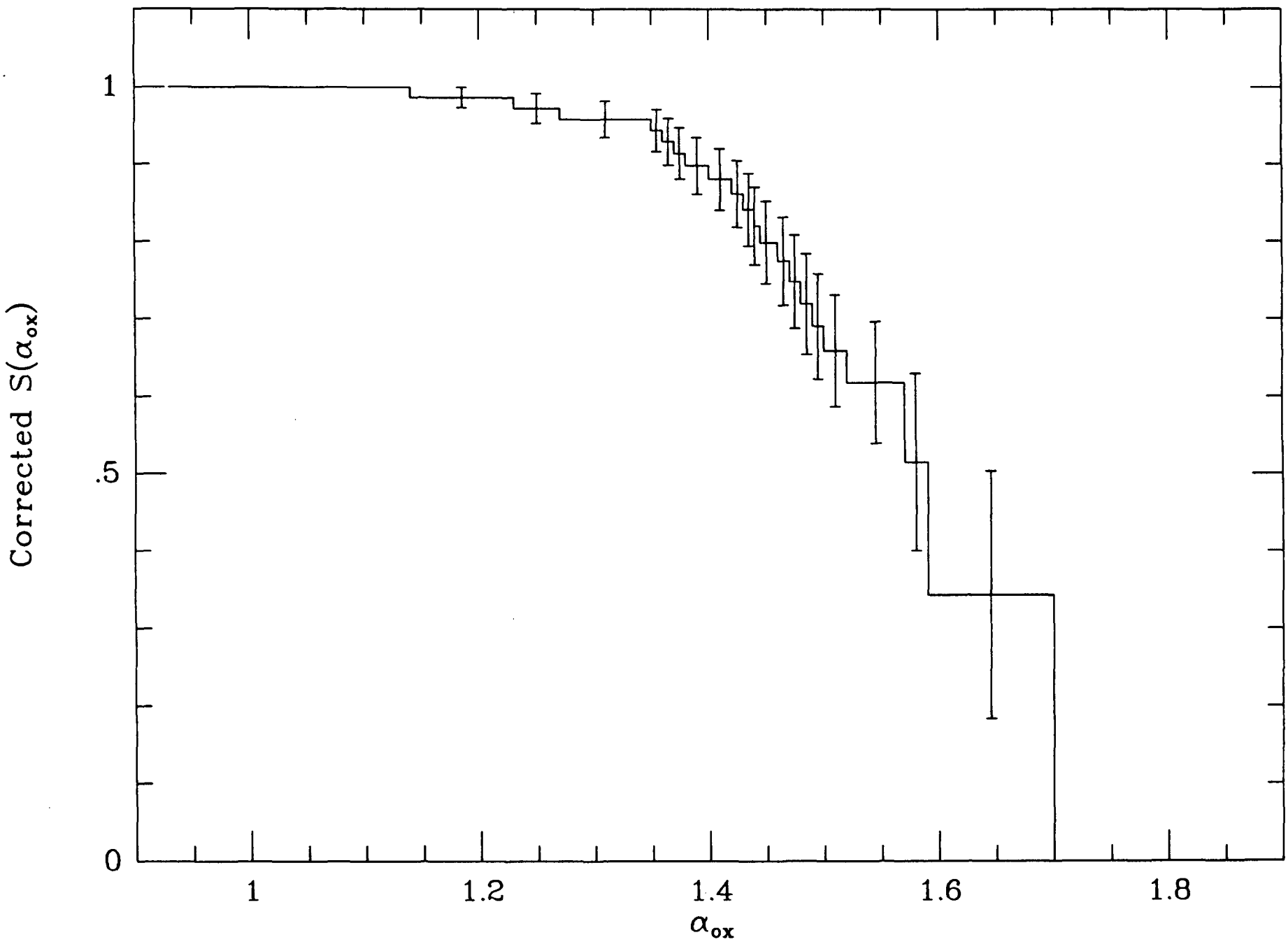

Figure 5